frontiers | Frontiers in Earth Science

TYPE Original Research
PUBLISHED 23 May 2023
DOI 10.3389/feart.2023.1064209

OPEN ACCESS

EDITED BY
Simon Large,
Natural History Museum, United Kingdom

REVIEWED BY
Veronica Oliveros,
University of Concepcion, Chile
Pura Alfonso,
Universitat Politecnica de Catalunya, Spain

*CORRESPONDENCE
José Piquer,
jose.piquer@uach.cl

RECEIVED 07 October 2022
ACCEPTED 05 May 2023
PUBLISHED 23 May 2023

CITATION
Piquer J, Fischer T, Torres F and Plissart G (2023), Spatiotemporal variability of magmatic products under a changing structural and tectonic context: a case study in the Andes of southern Central Chile.
Front. Earth Sci. 11:1064209.
doi: 10.3389/feart.2023.1064209

Spatiotemporal variability of magmatic products under a changing structural and tectonic context: a case study in the Andes of southern Central Chile

José Piquer*, Tomás Fischer, Francisco Torres and Gaëlle Plissart

Instituto de Ciencias de la Tierra, Universidad Austral de Chile, Valdivia, Chile

In a subduction setting, the type of magmatic products which reach the upper crust, and eventually the surface, depends on several variables, among which some of the most relevant are the tectonic regime, and the orientation of magma pathways relative to the predominant stress tensor. To better understand this relationship, we studied in detail an area of the Andes of southern Central Chile in which subduction-related magmatism has been active at least during the last 18 m.y. The relationship between high-angle faults and magmatism was studied, and the spatiotemporal variations on the stress tensor were analyzed. The chemistry of the different magmatic products was used to evaluate the magma "fertility", understood as its potential to form a giant porphyry-type deposit. The age of the studied units is constrained by new U-Pb zircon ages, complemented with previous geochronological studies. Three main high-angle fault systems are present: ~NW striking structures control the emplacement of plutonic bodies, while ~NE–ENE and N–NNE faults, more parallel to the prevailing orientation of σ_1 since the middle Miocene, control the emplacement of dike swarms and volcanic alignments. Regarding the geochemical characterization, a transition towards steeper REE patterns and higher fertility indices is observed in the earliest facies of the La Invernada Plutonic Complex (~15-14 Ma), coincident with a middle Miocene orogenic event described at this latitude by previous authors. The Pliocene La Resolana intrusions show higher magma fertility indices; however, they are still considerably lower than those typical for porphyry-forming magmas in the same Andean region. It is concluded that the contrasting fertility observed in coeval intrusions emplaced under the same tectonic context, cannot be explained by continental-scale processes; instead, they are related to differences in the local pathways of magma ascent through the crust. Fault systems which are miss-oriented relative to the predominant orientation of σ_1 appear to favor longer magma residence times, achieving a higher degree of differentiation and fertility in most cases crystalizing within the upper crust, while magmas ascending through more favorably oriented faults are more primitive, and often reach the surface forming stratovolcanoes and alignments of monogenetic vents.

KEYWORDS

Andes, magmatism, structural control, crustal thickness, fertility

1 Introduction

Understanding the flow of geofluids (magmas, hydrothermal fluids) through the crust, and their ultimate fate (including whether they reach the Earth's surface or not), constitute a major research topic which is also crucial for society, as it is directly related with phenomena such as active volcanism and the formation of mineral deposits. Multiple variables must be considered to tackle this challenge, particularly when different spatial and temporal scales are involved. This includes aspects related to the structural and tectonic context in which the geofluids evolve, and also the application of petrological studies to understand magma evolution. However, these two approaches are often considered separately. In this work, we attempt to integrate interpretations from structural geology and geochemical studies to understand the parameters which controlled the fate of geofluids in one particular Andean region, located within the high cordillera of the Maule Region in southern Central Chile (Figure 1). This area is ideally suited for this task, as it has been a focus of magmatism at least during the last 18 m.y., containing a large compositional variety of plutonic and subvolcanic intrusions and volcanic products. Besides, it has been proposed that in this Andean segment, margin-oblique structures inherited from the Andean basement play a first-order role over the geometry of volcanic chains and minor eruptive vents alignments (Salas et al., 2017), and would be responsible for the exceptional width of the Transitional Southern Volcanic Zone (34.5–37°S), while to the south the ~N–S volcanic arc is restricted and aligned over the margin-parallel Liquiñe–Ofqui Fault Zone (LOFZ; Cembrano et al., 1996).

2 Geological background

The study area is located within the Principal Andean Cordillera of the Maule Region, in southern Central Chile (~35°37′S–35°45′S; Figure 1). This Andean segment forms part of the Southern Volcanic Zone (SVZ) of the Andes; specifically, it corresponds to a continental-scale transition zone (Transitional Southern Volcanic Zone or TSVZ, López-Escobar et al., 1995) between the North and Central Southern Volcanic Zones (NSVZ and CSVZ; Figure 1). In the study area, within the TSVZ, the crust is estimated to have a thickness of ~45 km (Tassara and Echaurren, 2012). The Andean segment to the north, corresponding to the NSVZ, is characterized by a thicker continental crust, longer magma residence times (Hildreth and Moorbath, 1988; Cembrano and Lara, 2009) and the presence of giant porphyry-style Cu-Mo deposits, including the two largest known porphyry Cu-Mo systems in the planet (Rio Blanco-Los Bronces and El Teniente; Sillitoe, 2010). Towards the south, the CSVZ is characterized by a thinner crust, the absence of known porphyry systems, and by the presence of an active, arc-parallel fault system, the LOFZ, which strongly controls the locus of active volcanism (Cembrano et al., 1996).

The oldest rocks exposed in the Andean segment considered in this study correspond to Mesozoic volcanic, subvolcanic and sedimentary units, which crop out in the southwestern segment of the study area (Figure 1). The oldest stratigraphic unit is the Río Damas Formation, composed of Kimmeridgian sedimentary and volcanic deposits of continental environment (Klohn, 1960; González and Vergara, 1962). This unit is covered by the marine sediments of the Baños del Flaco Formation (Tithonian-Barremian; Klohn, 1960; González and Vergara, 1962). A subsequent shift to a continental environment is reflected by the red sandstones of the Colimapu Formation (Klohn, 1960; Barremian-Albian), which in turn is covered by the Late Cretaceous volcanic deposits of the Plan de los Yeuques Formation (Gonzalez and Vergara, 1962).

The Mesozoic units described before are covered and intruded by Cenozoic volcanic and intrusive rocks, which are associated with the establishment of the magmatic arc in the current Principal Cordillera. The oldest of these igneous units corresponds to a thick volcanic and volcano-sedimentary sequence, with ages ranging from the upper Eocene to the middle Miocene (Vergara et al., 1999; Cabezas et al., 2018), which have been interpreted as accumulated in a series of intra-arc, volcano-tectonic extensional basins (Vergara et al., 1999; Jordan et al., 2001; Charrier et al., 2002). The stratigraphic assignation of these rocks in our study area is controversial. Klohn (1960) assigned them to the Coya-Machalí Formation, which was defined in the Andean Precordillera at ~34.5°S. Later, Gonzalez and Vergara (1962) considered these sequences as part of the Abanico Formation, previously defined by Aguirre (1960) at 33-34°S. These two formational units (Coya-Machalí and Abanico) have been considered as equivalent by later works (e.g., Drake et al., 1976; Charrier et al., 2002), although Piquer et al. (2017) considered them as two separate units, based on U-Pb geochronology, which consistently show older ages for the Abanico Formation. Closer to the study area, in the Precordillera to the south of the Maule River valley, Vergara et al. (1999) defined the Colbún Formation, which was divided into two members; according to available radiometric ages, the lower member is coeval with the Abanico Formation, while the upper member strongly overlaps in age with the Coya-Machalí Formation. Finally, in the Principal Cordillera to the south of the study area (~36-39°S), equivalent Cenozoic volcanic and volcano-sedimentary rocks are assigned to the Cura-Mallín Formation (Suarez and Emparan, 1995), which is equivalent in age to both the Coya-Machalí Formation and the upper member of the Colbún Formation. The U-Pb ages reported by Cabezas et al. (2018) for volcanic rocks within our study area, fall within the age range of the upper member of the Colbún Formation, and of the Coya-Machalí and Cura-Mallín formations (Vergara et al., 1999; Piquer et al., 2017). Here we assign these rocks to the Colbún Formation, considering the proximity of our study area to its type locality, and the convenience of maintaining the local formational names for this type of syn-extensional volcanic and volcaniclastic deposits, which show a strong lateral variability in volcanic facies and depositional age.

The late Eocene-middle Miocene intra-arc basins were tectonically inverted during shortening episodes, which at this latitude begun in the middle Miocene (Astaburuaga, 2014; Tapia et al., 2015). Tectonic inversion caused strong folding of the Colbún Formation and equivalent units, and also of the previous Mesozoic sequences; fold axes and reverse faults predominantly strike NNE, and are E-vergent (Astaburuaga, 2014; Tapia et al., 2015). This period of mainly compressive tectonism during the middle to late Miocene has been associated with a proposed episode of flat subduction affecting the study area during this time (Payenia paleo-flat slab, Ramos et al., 2014), which would also be responsible of the exhumation of volcanic and intrusive rocks in

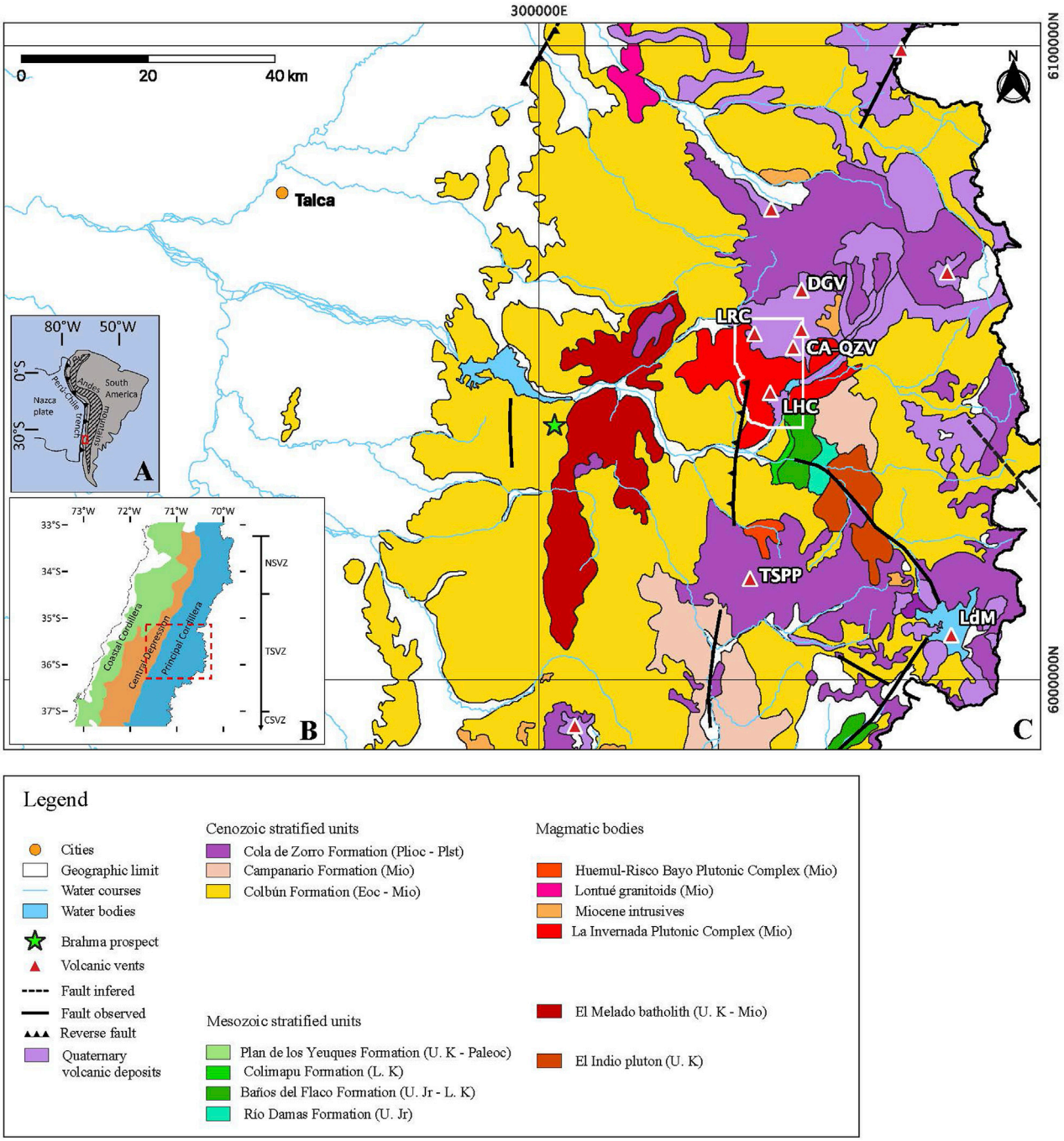

FIGURE 1
(A) Location of the study area (red rectangle) in South America. **(B)** Major morphostructural provinces and volcanic arc segmentation in southern Central Chile. Red dashed line highlights the area of **(C)**. **(C)** Regional geology of the Principal Cordillera of the Maule Region, modified from SERNAGEOMIN (2002); UTM coordinates. DGV = Descabezado Grande volcano; CA-QZV = Cerro Azul-Quizapu volcanic complex; LRC = La Resolana craters; LHC = Los Hornitos craters; TSPP = Tatara-San Pedro-Pellado volcanic complex; LdM = Laguna del Maule volcanic complex.

the study area, according to (U-Th)/He ages (Spikings et al., 2008). Coeval with this shortening event, a series of middle to late Miocene plutonic bodies were emplaced in the study area and surrounding regions, including intrusions such as the La Invernada pluton (Drake, 1976; Astaburuaga, 2014), the Huemul-Risco Bayo plutonic complex (Nelson et al., 1999; Schaen et al., 2017), and the intrusive units related to the Brahma porphyry Cu-Mo deposit (Díaz et al., 2020). The folded rocks of the Colbún and equivalent formations are unconformably covered by post-tectonic, flat-lying volcanic deposits: the mainly pyroclastic rocks of the late Miocene-early Pliocene Campanario Formation (Drake, 1976; Torres, 2021), and the basalts and basaltic andesites of the early Pliocene-early Pleistocene Cola de Zorro Formation (Gonzalez and Vergara, 1962; Drake, 1976).

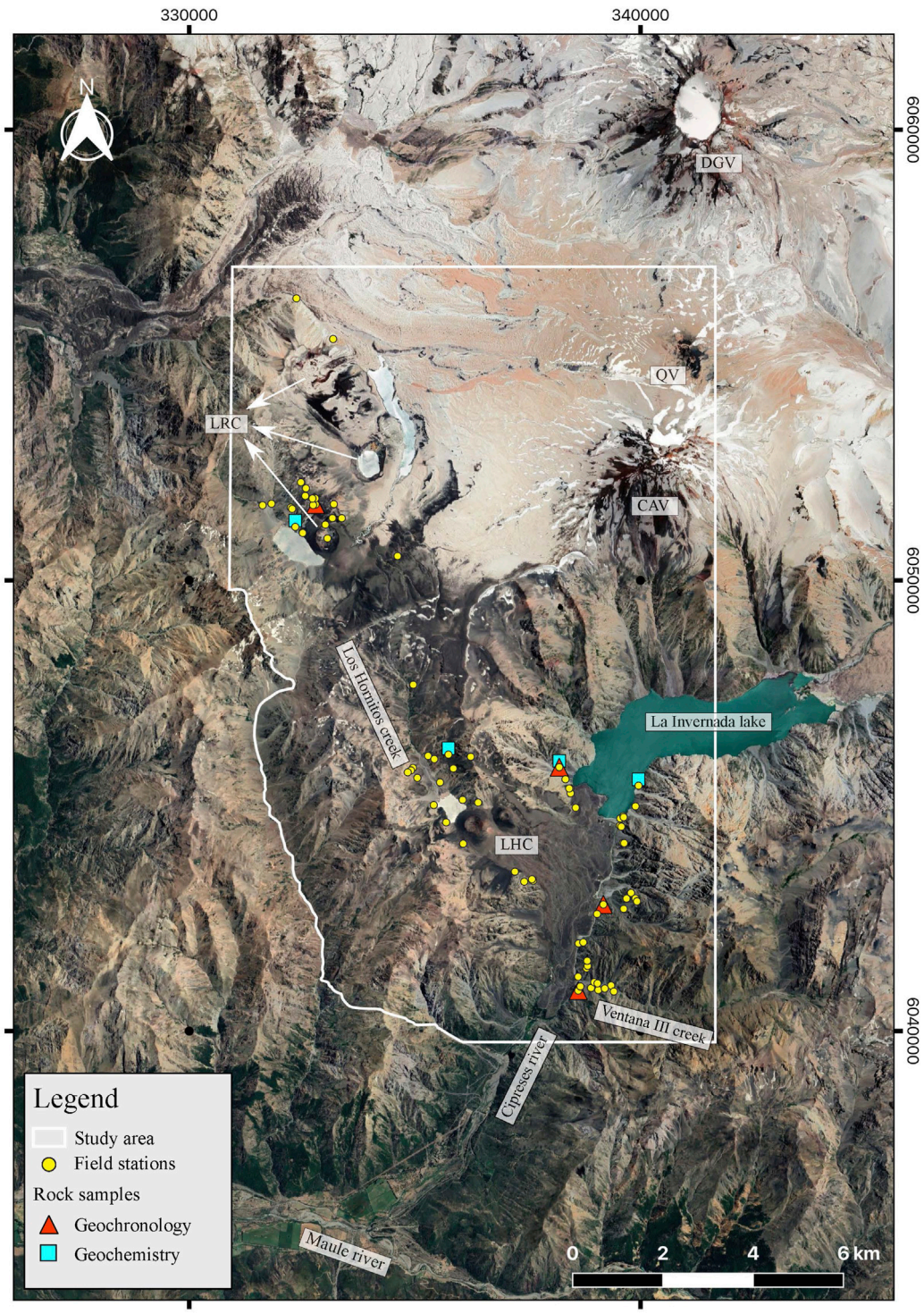

FIGURE 2
distribution of field stations and samples collected for this study.

Finally, all the aforementioned rock units are covered by the products of the active, Pleistocene-Holocene volcanic arc of the TSVZ. In the study area, they include the products of the Descabezado Grande Volcanic Complex (Figure 1), composed of the Descabezado Grande, Quizapu and Cerro Azul volcanoes, and also two major clusters of post-glacial monogenetic vents of basaltic-andesitic composition: the La Resolana and the Los Hornitos craters (Figure 1; Hildreth and Drake, 1992; Salas et al., 2017). At Los Hornitos, the age of the oldest vent was estimated as 1,148 years before present, through radiocarbon dating of paleosols (Contreras, 2019). Structural control on volcanism in the studied Andean segment, in particular for the Descabezado Grande Volcanic

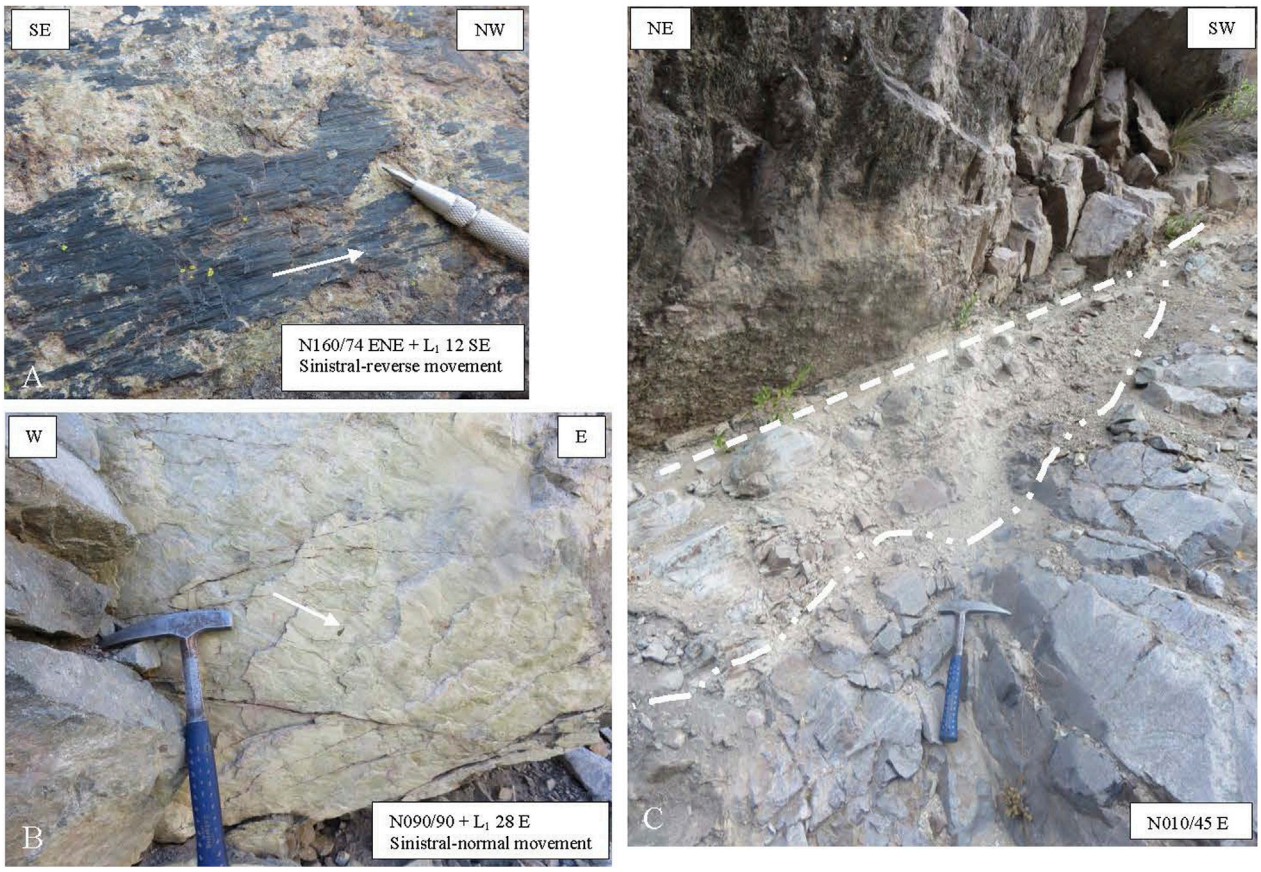

FIGURE 3
(A) Example of a fault plane containing syn-tectonic tourmaline fibers. **(B)** Example of a fault plane containing secondary R faults (RM criteria). **(C)** Dike of daci-andesite composition (lower part of the picture) emplaced along the Rio Cipreses fault, cross cutting a lithic tuff of the Plan de los Yeuques Formation. A brecciated damage zone is observed at the intrusive contact, evidence of post-magmatic reactivation of the fault.

Complex and the La Resolana and Los Hornitos craters, has been related to NNW- and NE-striking lineaments (Salas et al., 2017), interpreted as inherited pre-Andean structures, oblique to the NNE-trending axis of the magmatic arc and major reverse faults.

3 Methodology

Structural data was collected from 75 field stations (Figure 2). A total of 227 fault planes were measured, 132 of which contain reliable kinematic indicators. Other 42 structural elements were measured, including veinlets, dikes, intrusive contacts and magmatic foliation. For every fault plane, the strike and dip of the plane and the rake of striation were measured. When present, hydrothermal mineral infill was documented. The sense of movement of the fault planes was established through various kinematic criteria for brittle faults (Petit, 1987). The most common kinematic indicator was provided by steps in syn-tectonic hydrothermal minerals (Figure 3); also useful were the R-main (RM) and P-only criteria (Figure 3; Petit, 1987).

Representative samples of key igneous units were collected for geochemical and geochronological studies. Analytical work was focused on igneous units which did not count with geochemical and/or geochronological information reported in previous works. In four samples, whole-rock geochemical analyses were completed at the ALS Patagonia S.A. laboratory in Santiago, Chile and Lima, Perú. 13 major oxides and 12 metallic elements were analyzed through ICP- AES, while 42 minor and trace element concentrations were obtained through ICP-MS. The lithology of the analyzed samples was characterized by thin section description. Additionally, four samples were selected for U-Pb geochronological studies in magmatic zircons. The U-Pb zircon ages were obtained through a laser ablation equipment coupled with a Thermo Fisher ElementXR ICP-MS at the Geochronological Laboratory of SERNAGEOMIN (Chilean Geological Survey). The samples were first sieved and crushed, and then non-magnetic heavy minerals were concentrated using standard procedures. Zircons were detected and picked using UV light and a binocular lens. Cathodoluminescence images were obtained from the selected crystals, and they were mounted in epoxy glue briquettes for laser ablation analysis. In samples of intrusive rocks, 25 spots were selected at the crystal rims for laser ablation, using a Photon-Machines Analyte G2 193 nm excimer laser, with a spot diameter of 30 μm. In pyroclastic rocks, 30 spots were selected. U, Pb and Th concentrations were calculated using the reference zircon GJ-1 (Jackson et al., 2004), which was also used to normalize isotope

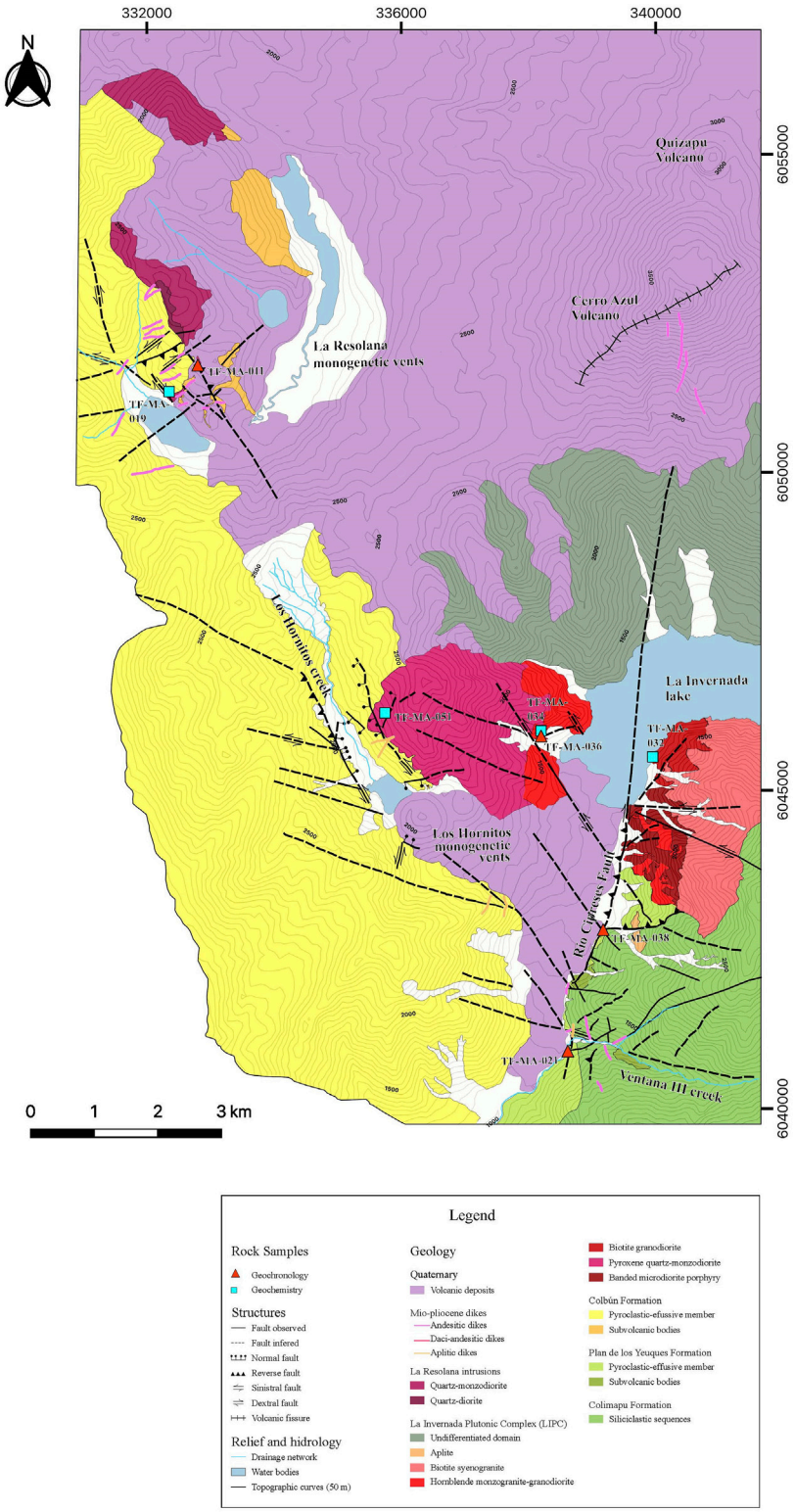

FIGURE 4
Geological map of the study area.

ratios; then, U-Pb ages corrected for common Pb were calculated (Williams, 1998). U-Pb zircon dating analytical data is provided as Supplementary Material S1.

Statistical, kinematic and dynamic analyses were completed on our structural database. The analyses were completed for the entire database, and also for various groups of faults, separated according

to two main criteria: the age of the lithological unit affected by faulting, and their assignation to specific structural blocks, defined as geographical areas characterized by a common lithology and deformation style. The software Stereonet (Allmendinger et al., 2012) was used to complete a statistical analysis to investigate the preferred orientation of faults, hydrothermal veins, dykes, intrusive contacts and magmatic flow banding. The kinematic analysis was completed using the Faultkin software (Marret and Allmendinger, 1990; Allmendinger et al., 2012), which allows to establish the orientation of the pressure and tension axis for each individual fault plane, and to calculate the average kinematic axes (shortening, stretching and intermediate axes) for a given fault population. Finally, the dynamic analysis was completed using the Multiple Inverse Method (MIM; Yamaji, 2000), with the aim of establishing the predominant paleo-stress tensor from the inversion of fault slip data, for different groups of faults. The advantage of the MIM software over other paleo-stress calculation methods, is that it allows to distinguish between homogeneous (active under one single stress state) and heterogenous (with reactivations under different stress states) fault populations. For the latter case, it is possible to estimate the orientation and geometry of the different prevailing stress tensors. A stress state is defined by the orientation of the three principal stresses (σ_1, σ_2 and σ_3) and by the stress ratio $\phi = (\sigma_2-\sigma_3)/(\sigma_1-\sigma_3)$, which defines the geometry of the stress ellipsoid.

4 Results

4.1 Characterization of intrusive units and their host rocks

Detailed field mapping and petrographic characterization were completed for the intrusive units cropping out at La Invernada and La Resolana and their host rocks (Figure 4). The intrusive rocks at La Invernada have previously been treated as a single pluton, but here we consider them as a plutonic complex (La Invernada Plutonic Complex, LIPC), subdivided into six main facies (Figure 4). At La Resolana, in turn, two main intrusive units have been recognized.

4.1.1 Host rocks

4.1.1.1 Colimapu Formation

This is the oldest host rock of the Miocene intrusive units in the study area. It is composed of a sequence of continental, reddish-colored, medium-to coarse-grained sandstones, matrix-supported red conglomerates, discrete lenses of calcareous shales and thin bioclastic intercalations containing fragments of bivalves and gastropods. Within the study area, this unit is characterized by a NNW strike, dipping at high angles to the W, in some cases being sub-vertical. The unit is intruded by a set of andesitic dikes, parallel to the bedding planes. The age of these dikes is unknown, although it is likely that they are related to the late Cretaceous volcanism of the Plan de los Yeuques Formation (see below). The established age range of Colimapu Formation, base on U-Pb dating of detrital zircons and stratigraphic relationships, is Barremian–Albian (Early Cretaceous; CCharrier et al., 2002; Astaburuaga, 2014).

4.1.1.2 Plan de los Yeuques Formation

This Mesozoic unit has not been recognized previously in the study area; all the volcanic rocks to the west of the Colimapu Formation have previously been assigned to Cenozoic formations (e.g., Astaburuaga, 2014).

The rocks belonging to this unit conformably overly the Colimapu Formation, and are in fault contact to the west with the Colbún Formation. Lithologically, the Plan de los Yeuques Formation is composed of intercalations of massive beds of felsic, crystal- and lithic-rich ignimbrites of grey-green color containing fragments of plagioclase, K-feldspar, quartz and vitric fiamme; lithic- and pumice-rich tuffs of reddish color; porphyritic, daci-andesitic lava flows; and resedimented, volcanogenic sedimentary deposits. This volcanic sequence is intruded by subvolcanic stocks and dikes. The intrusive bodies vary in texture and composition; they can be classified as medium-to coarse-grained porphyritic andesites; micro-phaneritic, hornblende-bearing tonalite porphyries; and micro-phaneritic, hornblende-bearing quartz-diorites (Figure 5). The dikes differ from the ones emplaced in the Colimapu Formation, in that those cutting across the Plan de los Yeuques Formation are discordant to the bedding planes. The new observation of peperites developed at the contacts between some of the coarse-grained andesite porphyries and volcano-sedimentary deposits (Figure 5), suggests that at least some of the subvolcanic intrusions are coeval with volcanic activity, and would thus pertain to the same Plan de los Yeuques Formation.

Hydrothermal alteration is sometimes intense in these rocks, especially in areas close to the contact with the nearby LIPC (La Invernada Plutonic Complex). Plagioclase are commonly replaced by sericite, chlorite and calcite, while hornblende is replaced by chlorite. Veins of epidote-chlorite-calcite-tourmaline infill are also common. Vein width is commonly 1–3 mm. The frequency of the veins is variable; in the most intensely altered areas, more than 10 veins per meter can be present, and the original rock texture is obliterated.

Drake (1976) reported K-Ar ages in hornblende and biotite for the subvolcanic intrusions described before, which yielded 7.0 ± 0.5 and 6.3 ± 0.1 Ma respectively, and consequently were assigned to the LIPC. To test this late Miocene age, we obtained LA-ICP-MS U-Pb zircon ages for one of the tonalitic subvolcanic intrusions, and also from a crystal- and lithic-rich pyroclastic deposit (Supplementary Table S1). For the latter, an age of 84.8 ± 1.0 Ma (Late Cretaceous; Figure 6, sample TF-MA-021) was obtained. For the subvolcanic intrusion, three different age populations were identified (Figure 6, sample TF-MA-038), probably reflecting zircon inheritance and the incorporation of fragments of the host rock. The two youngest ages, 90.6 ± 0.8 and 94.7 ± 1.1 Ma, probably reflect the crystallization age range. Even with this important degree of uncertainty, the calculated ages allow us to assign a Late Cretaceous age to the subvolcanic intrusions, broadly coeval with the Late Cretaceous volcanism in the area, discarding its assignation to the LIPC.

Similar felsic tuffs assigned to the Plan de los Yeuques Formation are recognized in various segments of the Principal Cordillera of the Maule Region, overlying the red-colored, continental sedimentary deposits of the Colimapu Formation (Klohn, 1960; González and Vergara, 1962). However, our radiometric ages are slightly older than the age range estimated

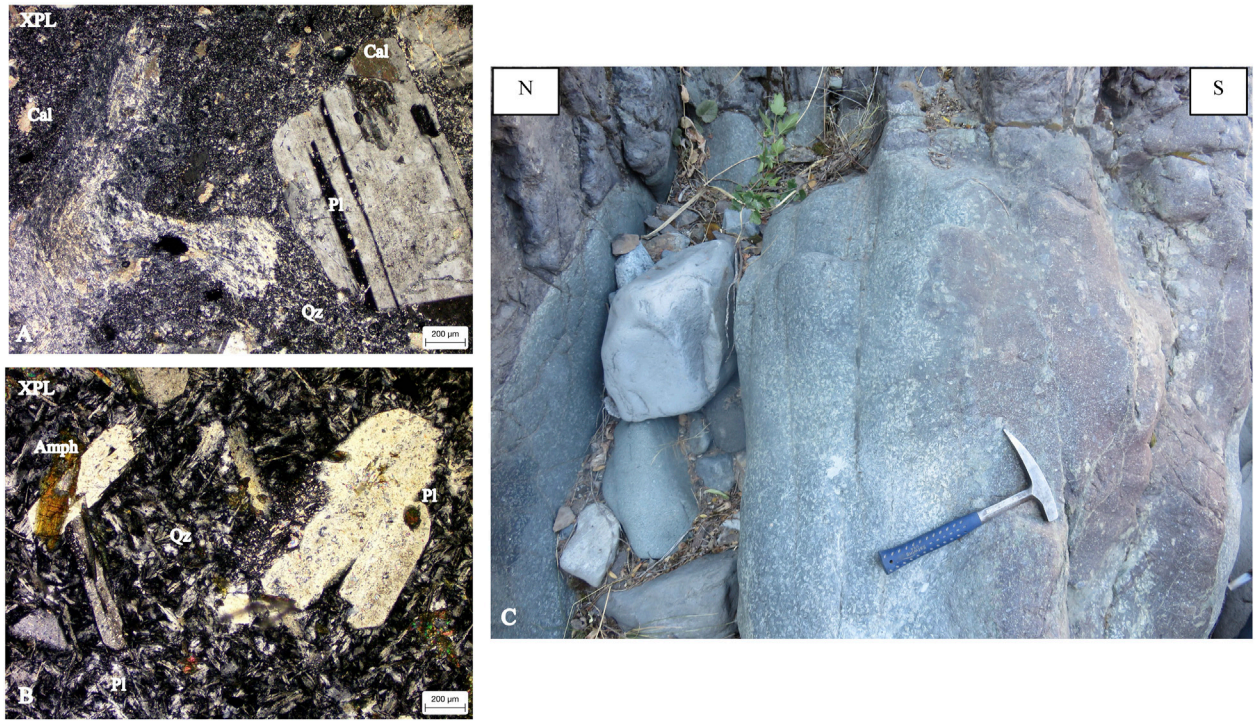

FIGURE 5
(A) Vitro-crystalline tuff of the Plan de los Yeuques Formation. It contains plagioclase crystals (Pl) in a matrix composed of volcanic glass and microcrystalline quartz (Qz). Later replacement by calcite (Cal) is common. **(B)** Cross-polarized microphotograph of a subvolcanic intrusion of the Plan de los Yeuques Formation. It contains plagioclase (Pl) phenocrysts with reabsorption textures and less common amphibole (Amph) phenocrysts, in a groundmass composed of plagioclase and quartz (Qz). **(C)** Field photograph of a coarse-grained andesite (left) intruding a tuffaceous volcaniclastic layer; the contact is strongly irregular, diffuse and disaggregated, and is interpreted as a peperite.

for the Plan de los Yeuques Formation by previous works (~81-67 Ma; Muñoz et al., 2018), and coeval with the informally defined "Brownish-reddish clastic unit", BRCU (Charrier et al., 1996; Muñoz et al., 2018). The latter corresponds to a sequence of red continental sedimentary deposits, mostly sandstones, lithologically very similar to the Colimapu Formation, but younger in age (Muñoz et al., 2018). Given that (1) the Late Cretaceous pyroclastic deposits recognized here are identical to the rocks assigned to the Plan de los Yeuques Formation elsewhere in this Andean segment, (2) their stratigraphic position overlying the Colimapu Formation, and (3) the absence of red beds that are characteristic of the BRCU, we prefer to keep the stratigraphic assignation of these rocks to the Plan de los Yeuques Formation, and propose that the initiation of this Late Cretaceous volcanic episode occurs at least at 85 Ma.

4.1.1.3 Colbún Formation

The western part of the study area is dominated by outcrops of this unit (Figure 4). The contact with the Plan de los Yeuques Formation to the east is covered by fluvial deposits of the Cipreses River and recent lava flows related to the Los Hornitos monogenetic vents. It is inferred that the contact could be defined by a N- to NNE-striking, high-angle, E-vergent reverse fault, interpreted as an inverted normal fault, as several fault planes with this orientation and sense of movement crop out along the Cipreses River valley.

Lithologically, this unit is characterized in the study area by various types of volcanic products, intruded by subvolcanic stocks and dikes. The volcanic deposits can be subdivided into two main packages. One of them crop out in the area of La Resolana, and it is composed of daci-andesitic pyroclastic deposits, mainly crystal- and pumice-rich ash and lapilli tuffs. The other package crops out to the west of the Los Hornitos Creek (Figure 4), and it is composed of porphyritic lava flows and volcanic breccias of andesitic composition, intercalated with volcanogenic sandstones and lithic-rich lapilli tuffs. The subvolcanic bodies correspond to porphyritic andesites which crop out mainly in the area of La Resolana. They are cut by felsic dikes related to the La Resolana intrusions.

These rocks are affected by contact metamorphism and hydrothermal alteration, related to the emplacement of the LIPC and the La Resolana intrusions. Contact metamorphism is mainly reflected in the presence of fine-grained secondary biotite in the groundmass and strong disseminated magnetite, while hydrothermal alteration corresponds mainly to epidote, chlorite, actinolite and sericite, which occur in veins and as selective replacements of primary phenocrysts.

Cabezas et al. (2018) presented two new U-Pb zircon ages in volcanic rocks, from samples collected in the vicinity of the study area (~1.3 km to the south), in the western flank of the Los Cipreses River valley. The resulting ages are 14.12 ± 0.17 and 13.84 ± 0.26 Ma. Another sample, ~5 km to the south, yielded 18.07 ± 0.27 Ma. Based on this, it is possible to assign a middle Miocene age to the Colbún Formation in the study area.

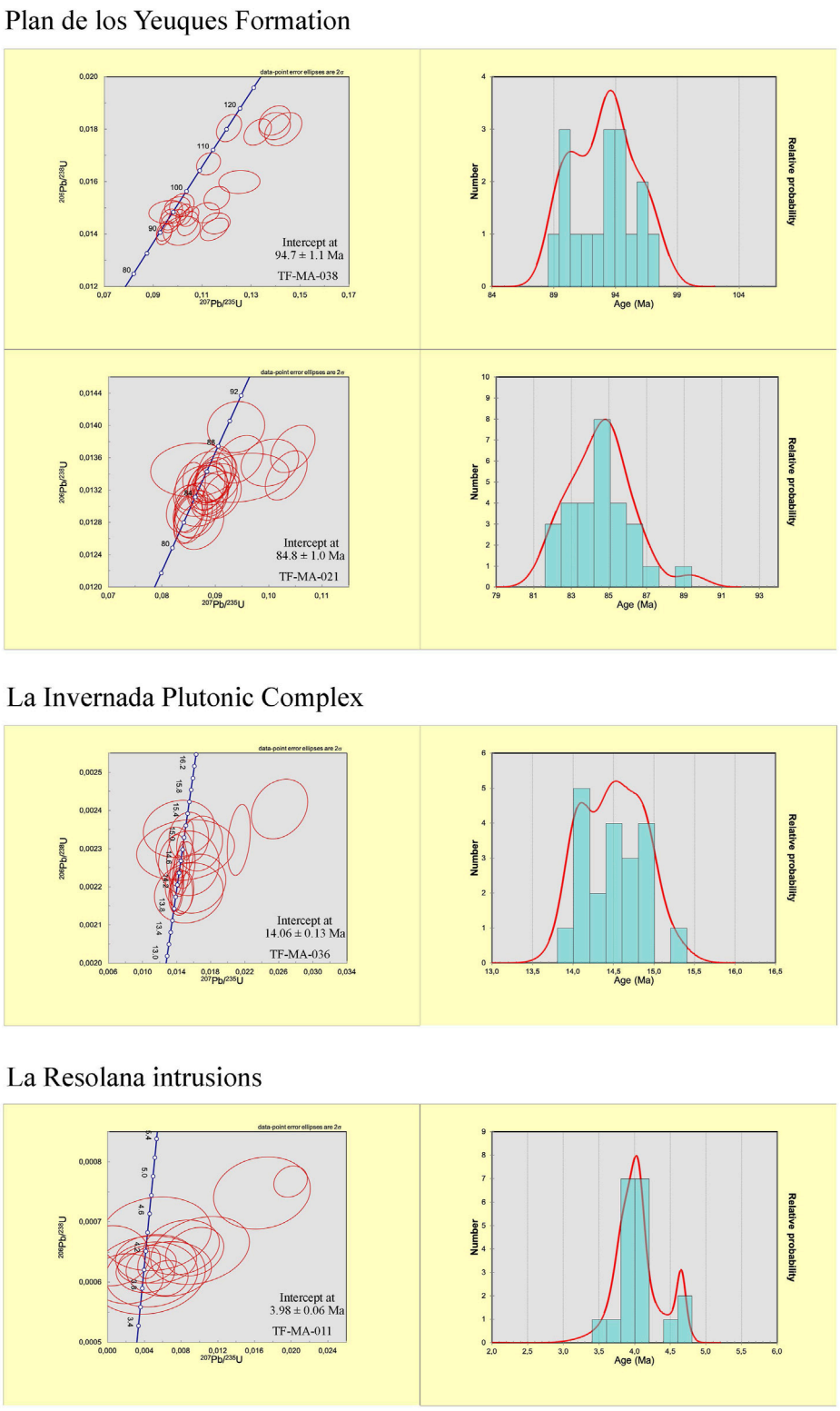

FIGURE 6
U-Pb concordia diagrams and probability plots for the four samples in which U-Pb zircon ages were obtained.

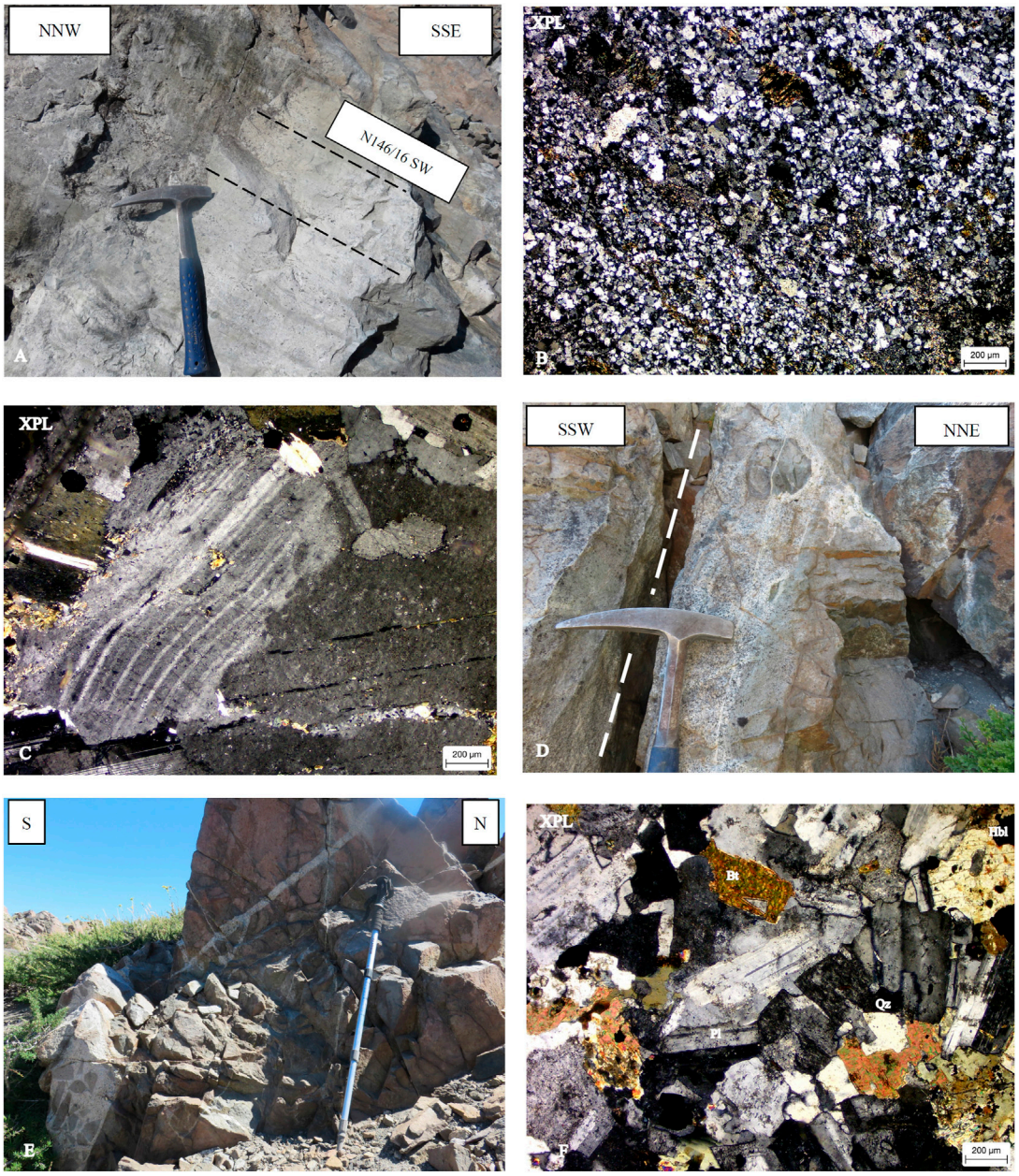

FIGURE 7
(A) Flow banding observed in monzogranite facies of the LIPC. **(B)** Microphotograph of the flow-banded monzogranite. Incipient bands of quartz, plagioclase and white mica are observed. **(C)** Intracrystalline deflection of plagioclase, evidence of ductile deformation. **(D)** Biotite syenogranite of the LIPC, cross-cutting a quartz-monzodiorite in the Los Hornitos area. The contact is faulted and strikes NW. **(E)** Contact between quartz-monzodiorite (left, brecciated) and quartz-diorite at La Resolana. A magmatic breccia is developed at the contact, with quartz-diorite clasts in a quartz-monzodiorite matrix. Quartz-monzodiorite dikes are also observed, intruding the quartz-diorite. **(F)** Microphotograph of the biotite and pyroxene quartz-monzodiorite at La Resolana. Pl = plagioclase, Qz = quartz, Bt = biotite, Hbl = honblende.

4.1.2 La Invernada plutonic complex

4.1.2.1 Banded microdiorite porphyry and biotite monzogranite

These two closely interrelated lithologies crop out in an area of ~0.76 km^2 at the SE margin of the La Invernada Lake. Its southernmost outcrops intrude the Plan de los Yeuques Formation (Figure 4). Around 80% of the surface exposures of this unit correspond to a mesocratic microdiorite porphyry, composed of plagioclase phenocrysts within a microcrystalline groundmass of plagioclase and minor quartz and potassium feldspar. Feldspars are strongly altered to sericite-quartz, while mafic minerals are commonly replaced by fine-grained biotite and magnetite. Veinlets of fine-grained sericite and of epidote-albite-chlorite are common. The microdiorite porphyry is intercalated with bands of leucocratic biotite monzogranite, with which it displays gradational contacts. This lithology has a fine-

grained phaneritic texture, sometimes slightly inequigranular, and is composed of quartz, potassium feldspar, plagioclase and biotite. It is affected by strong alteration to sericite and quartz. The monzogranite shows a characteristic flow banding; the bands have widths of centimeters to tens of centimeters, and their strike is NW, with shallow dip and varying dip directions, from 16°SW to 36°NE (Figure 7). Banding is compositional, defined by varying quartz contents, and it is also reflected in the orientation of plagioclase, biotite and muscovite crystals (Figure 7).

There are no radiometric ages for any of these lithologies but based on contact relationships and their very strong hydrothermal alteration, they are interpreted as the earliest facies of the LIPC.

4.1.2.2 Pyroxene quartz-monzodiorite

This unit crop out in an area of 4.65 km^2 to the NE of the Los Hornitos Creek (Figure 4), and it is surrounded by a halo of iron oxides in its host rock (mainly hematite and goethite), probably the product of oxidation and leaching of pyrite formed by contact metamorphism. The rock is mesocratic with a phaneritic texture, fine-to medium-grained, composed of tabular plagioclase crystals, pyroxene, and minor potassium feldspar and quartz. Pyroxenes are altered to chlorite, epidote and actinolite, while plagioclase is selectively altered to sericite and clays. Veinlets of chlorite and calcite are also present.

This unit has no radiometric ages, although contact relationships indicate that it is older than the more felsic granodiorite, monzogranite and syenogranite facies.

4.1.2.3 Biotite granodiorite

This unit crops out at the eastern margin of the La Invernada Lake, covering an area of ~0.49 km^2. It corresponds to a leucocratic, holocrystalline, phaneritic rock, with medium grain size, and it is composed of tabular plagioclase crystals, potassium feldspar, quartz and biotite, with minor clinopyroxene and hornblende. Microtextural evidence for ductile state deformation is present (Figure 7). Hydrothermal alteration corresponds mainly to secondary biotite, actinolite and chlorite partially replacing mafic minerals.

Cabezas et al. (2018) reported a U-Pb zircon age for this unit, which yielded 14.19 ± 0.12 Ma.

4.1.2.4 Hornblende monzogranite-granodiorite

This intrusion crops out at the SW margin of the La Invernada Lake, and also to the east of the upper Cipreses River valley. In between, it is covered by the recent lava flows of Los Hornitos (Figure 4). The rock is leucocratic with a phaneritic texture, and a fine to medium grain size. It is composed of tabular plagioclase, potassium feldspar, quartz and hornblende, with very minor clinopyroxene. There is weak sericite and epidote alteration in plagioclase, and hornblende is partially replaced by actinolite, chlorite and magnetite. The rock is also cut by epidote-chlorite veinlets with albite halos.

A new LA-ICP-MS U-Pb zircon age was obtained for this unit. The sample (TF-MA-036, Figure 6) was collected at the western shore of the La Invernada Lake. Two distinct age groups are present, the youngest of which is interpreted as the final crystallization age of this pluton, calculated as 14.06 ± 0.13 Ma. This result discard the 7.1 ± 0.2 Ma K-Ar age reported by Drake (1976) for this unit, and it is within error of the U-Pb age reported by Cabezas et al. (2018) for the biotite granodiorite.

4.1.2.5 Biotite syenogranite

This intrusion crop out at the eastern part of the study area, covering an area close to 3.2 km^2, cross-cutting Mesozoic stratigraphic units and the older facies of the LIPC (microdiorite porphyry-biotite monzogranite, biotite granodiorite and hornblende monzogranite). More to the west, to the north of the Los Hornitos craters, a dike of biotite syenogranite cuts across the pyroxene quartz-monzodiorite (Figure 7). It corresponds to a leucocratic rock with a phaneritic texture, fine to medium grained, composed mainly of quartz and potassium feldspar, with minor plagioclase, biotite and hornblende.

Astaburuaga (2014) reported a U-Pb zircon age for this unit in the area located to the north of the Los Hornitos craters, obtaining 12 ± 0.7 Ma.

4.1.3 La Resolana intrusions

4.1.3.1 Pyroxene quartz-diorite

This unit shows an apparent NNW elongation (Figure 4), with a long axis of ~1 km. It is melanocratic, fine-grained, and composed mainly of plagioclase and pyroxene, with minor quartz, potassium feldspar and biotite. There is weak sericite alteration of feldspars, while actinolite, chlorite and magnetite partially replace pyroxenes. The unit is cross-cut by chlorite veinlets.

There are no radiometric ages for this unit, but from cross-cutting relationships, it is considered the oldest of the La Resolana intrusions.

4.1.3.2 Biotite and pyroxene quartz-monzodiorite

This is the largest of the La Resolana intrusions (Figure 4); it has a NNW elongation, and develops magmatic breccia zones at the contact with the older pyroxene quartz-diorite (Figure 7). The rock is leucocratic, fine-to medium-grained, with a mineralogy dominated by plagioclase, pyroxene and biotite, with minor hornblende, quartz and potassium feldspar (Figure 7). Plagioclase is altered to clays, while pyroxene shows weak chlorite alteration.

One sample from this unit was selected for U-Pb zircon dating (sample TF-MA-011, Figure 6). 16 of the 21 analyses indicate a crystallization age of 3.98 ± 0.06 Ma.

4.1.4 Geochemistry of cenozoic intrusions

Four samples were analyzed to characterize the whole-rock geochemistry of the main intrusive facies of the LIPC and the La Resolana intrusions. The LIPC units analyzed correspond to the pyroxene quartz-monzodiorite, the biotite granodiorite and the hornblende monzogranite-granodiorite, while for La Resolana the analyzed sample comes from the biotite and pyroxene quartz-monzodiorite.

The geochemical results are presented in the Supplementary Material S2. Geochemical classifications for the analyzed units are shown in Figure 8. It is observed that the geochemical classification of the samples in the TAS diagram differs slightly from the classification based on microscopic modal mineralogy, while in the AFM diagram all the samples plot within the calc-alkaline field.

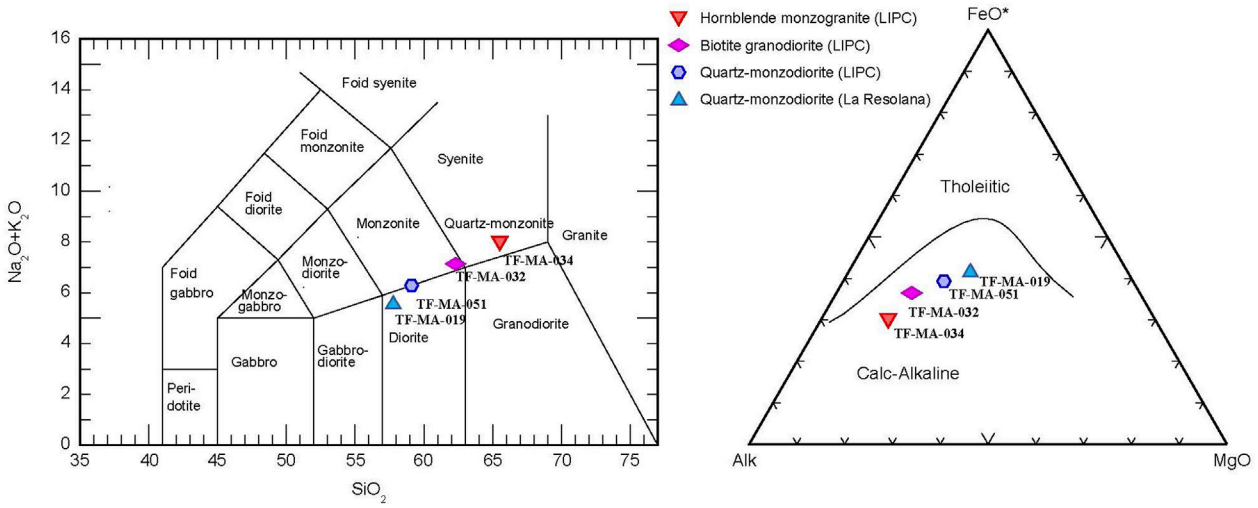

FIGURE 8
Geochemical classification diagrams for the analyzed rocks of the LIPC and the La Resolana intrusions. The left panel shows a TAS diagram for plutonic rocks (Le Maitre et al., 2002), while the right panel shows an AFM diagram (Irvine and Baragar, 1971).

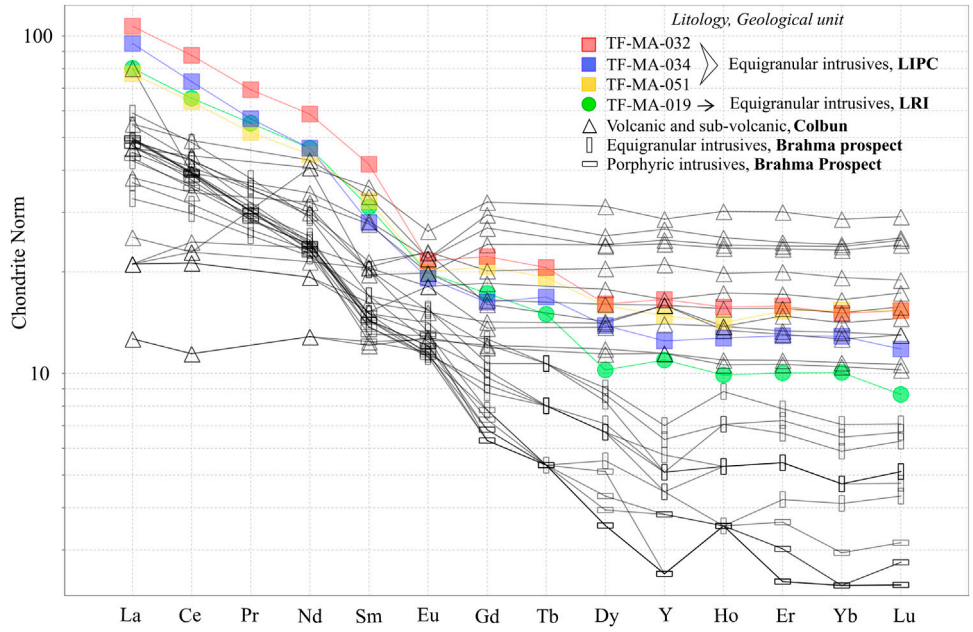

FIGURE 9
Chondrite-normalized (Sun and McDonough, 1989) REE diagram for rocks of different Miocene-Pliocene igneous units of the Principal Cordillera of the Maule region.

The three analyzed LIPC units show a similar pattern in a chondrite-normalized REE diagram (Figure 9), with a noticeable depletion in HREE, although the slope in the diagram is slightly steeper for the most differentiated of the three intrusions (hornblende monzogranite). The La Resolana quartz-monzodiorite, in turn, has a clearly stronger HREE depletion than the three analyzed facies of the LIPC, irrespective of their SiO_2 content. It is also observed that the two earliest facies of the LIPC display a more pronounced negative Eu anomaly than the later monzogranite facies and the quartz-monzodiorite of La Resolana. This was quantified using the formula proposed by Lu et al. (2016), in which a value of 1 represents no Eu anomaly. The values calculated for the LIPC quartz monzodiorite and granodiorite were 0.77 and 0.71 respectively, while for the monzogranite it is 0.9, and for the La Resolana quartz monzodiorite 0.86.

4.2 Structural mapping

The main fault systems observed in the study area are shown in Figure 4.

4.2.1 WNW-striking fault system

This fault system is the most represented in the study area. Several individual faults and morphological lineaments were observed in the eastern flank of the Cipreses River valley (to the south of the La Invernada Lake), and also towards the west, between the La Invernada Lake and Los Hornitos Creek. The faults present high dip angles, and the dip direction alternates between NNE and SSW. The fault cuts through Mesozoic stratigraphic units, and through Cenozoic volcanic and intrusive rocks. A syenogranite intrusion from the LIPC with a WNW elongation, was emplaced along one of these faults (Figure 7). The predominant sense of movement of this fault system is sinistral, although dextral, normal and reverse displacements were also documented (Figure 4).

4.2.2 NNW-striking fault system

This fault system is parallel to the Los Hornitos Creek, represented by several individual faults in that area; it was also recognized in the middle course of the Cipreses River, around the Ventana III Creek (Figure 4). It cuts through the Colimapu, Plan de los Yeuques and Colbún formations, and also through facies of the LIPC. The La Resolana intrusions are emplaced along this fault system, and its NNW-trending elongation is parallel to the strike of the faults. Kinematically, individual faults belonging to this fault system show sinistral movements in the areas of the Ventana III Creek, Cipreses River and La Invernada Lake, while at La Resolana, both sinistral and dextral displacements were observed. A particular situation was observed at Los Hornitos Creek, where a normal sense of movement prevails, with a minor population of faults showing reverse displacements.

4.2.3 NE-to ENE-striking faults

Two main fault system with this orientation have been recognized: one in the eastern margin of the Cipreses River valley, mainly around the Ventana III creek, and another around the La Resolana ponds (Figure 4). The faults dip at high angles, and the dip direction is predominantly to the NW at Cipreses and Ventana III, while at La Resolana it is to the SE. One segment of this fault system puts in contact the Colimapu and Plan de los Yeuques formations in the eastern flank of the Cipreses River valley. Individual faults are characterized by well-developed fault gauge in the fault cores. Several dikes are emplaced along them, and the Los Hornitos vents are also aligned on an ENE trend. Dextral sense of movements predominate in this fault system, although sinistral, reverse and normal displacements were also observed, indicating a complex reactivation history.

4.2.4 Rio Cipreses fault

Although N- to NNE-striking faults are not common in the study area, a major west-dipping, high-angle reverse fault with a minor dextral component was observed along the Cipreses River valley (Figure 4). The fault constitutes the boundary between Cenozoic rocks of the Colbún Formation to the west (hanging wall) and Mesozoic units to the east (footwall). As the rocks in the hanging wall are younger, we interpret this structure as an inverted normal fault, consistent with its high dip angle. Smaller faults with the same NNE strike were observed at Los Hornitos, with a predominant normal sense of movement. Dikes of various compositions were observed emplaced along the Rio Cipreses fault.

4.3 Statistical, kinematic and dynamic analysis

The fault plane database was analyzed to establish the preferred orientations of fault planes in the study area and in specific structural blocks, and kinematic and dynamic analyses were completed to better understand the conditions under which faulting occurred in different sectors and lithologies of the study area.

When the whole fault plane database is considered (N=227), it is possible to observe three preferred orientations (Figure 10), which are in agreement with the predominant orientation of large-scale faults represented in our geological map (Figure 4). The largest group shows WNW strikes, the second group shows NNW strikes, while a third noticeable population strikes NE to ENE. For all three groups, it is not possible to distinguish a preferred dip direction (Figure 10). When only faults with kinematic indicators are considered (N=132), the three main preferred strikes are preserved, although some preferred dip directions are apparent: WNW-striking faults dip preferentially to the NNE, NNW-striking faults tend to dip towards the WSW, while NE striking faults dip preferentially to the NW.

The kinematic analysis for the 132 fault planes with kinematic information, shows a very high dispersion of pressure and tension axes, evidencing a highly heterogenous deformation (Figure 10). This heterogeneity is confirmed by the results of the dynamic analysis using the Multiple Inverse Method (Figure 10), which shows that fault activation occurred under multiple stress states. The largest cluster (cluster A in Figure 10) is characterized by an E-to ESE-trending σ_1, and σ_3 varying from subhorizontal NNW to subvertical, with ϕ values close to 0 (σ_2 and σ_3 of similar magnitude). This is typical of a transpressive tectonic regime. A second cluster (cluster B in Figure 10) is defined by a σ_1 trending NE and commonly plunging at high angles, although with a high variability, and a subhorizontal, NW-trending σ_3, with ϕ values between 0.5 and 1. This can be considered a transtensional regime. Finally, a third cluster (cluster C in Figure 10) can be defined as a purely strike-slip regime, with σ_1 and σ_3 subhorizontal and trending N and E respectively, and ϕ values close to 0.5.

4.3.1 Analysis by structural blocks

To complete this analysis, the study area was subdivided into five structural blocks (Figure 11), each one characterized by specific lithologies and deformation styles.

4.3.1.1 La Resolana structural block

This block is located to the southwest of the volcanic plateau dominated by the Descabezado Grande and Cerro Azul stratovolcanoes (Figure 11). It contains the La Resolana monogenic vents, however, faults were not observed cutting through them. A total of 61 fault planes were measured in this structural block, most of them cutting through rocks of the Colbún Formation; only 8 fault

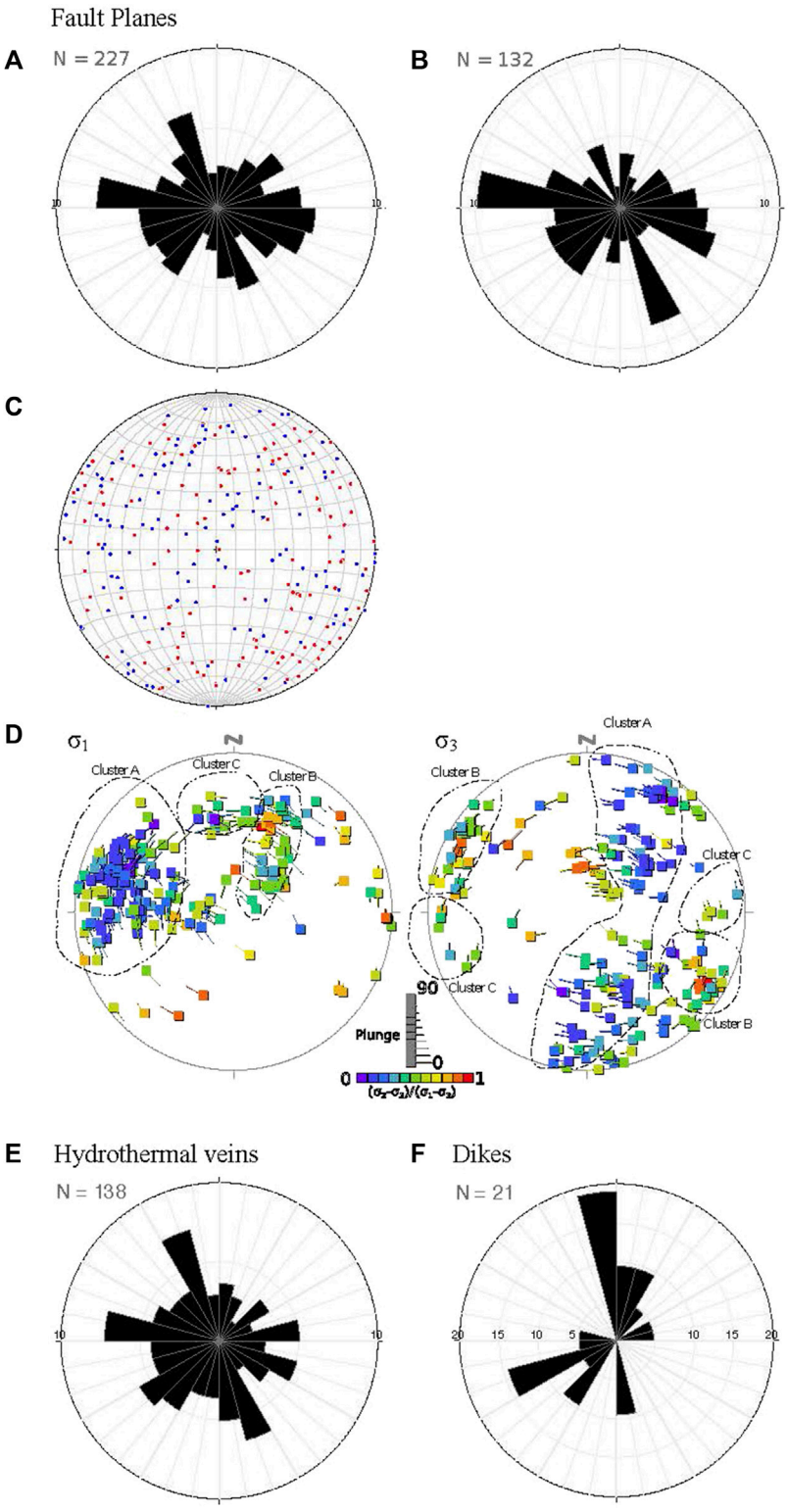

FIGURE 10
(A) Rose diagram for the strike (using the right-hand rule) for the 227 fault planes measured. **(B)** Rose diagram for the 132 fault planes which contained reliable kinematic indicators. **(C)** Lower hemisphere, equal-area projection of the P and T axes for all the fault planes with kinematic information, shown as blue and red dots respectively. **(D)** Lower hemisphere, equal-area projections of the calculated orientations of σ_1 and σ_3 for subgroups of fault-slip data using the Multiple Inverse Method. **(E)** Rose diagram for the strike of 138 hydrothermal veins. **(F)** Rose diagram for the strike of 21 dikes.

10.3389/feart.2023.1064209

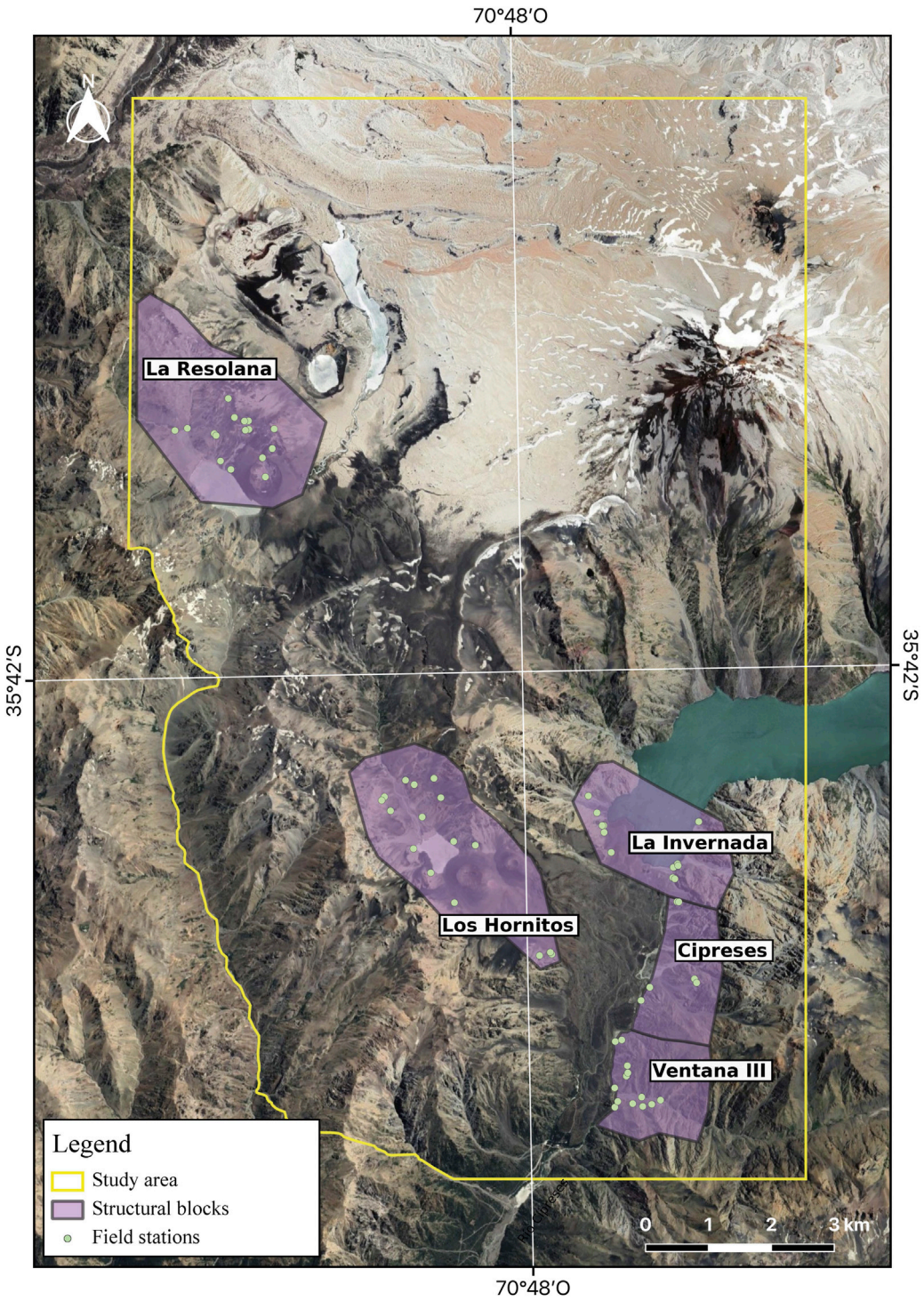

FIGURE 11
Distribution of the structural blocks into which the study area was subdivided.

planes were observed cross-cutting rocks of the La Resolana intrusions. Fault planes with a WNW strike predominate, dipping to the SSW (Figure 12). They are followed by faults striking NE and NNW.

The kinematic analysis (Figure 12), completed for 43 fault planes with reliable kinematic information (6 of them cutting through La Resolana intrusions) shows that deformation within this block is heterogenous, with an apparently random distribution of P and T axes. This heterogeneity is confirmed by the dynamic analysis, which shows that the principal stresses define several different stress states (Figure 12). Cluster A in Figure 12 corresponds to a stress state characterized by NE-trending σ_1, SE-trending σ_3 (both plunging at low angles) and ϕ values close to 0. Cluster B is characterized by high

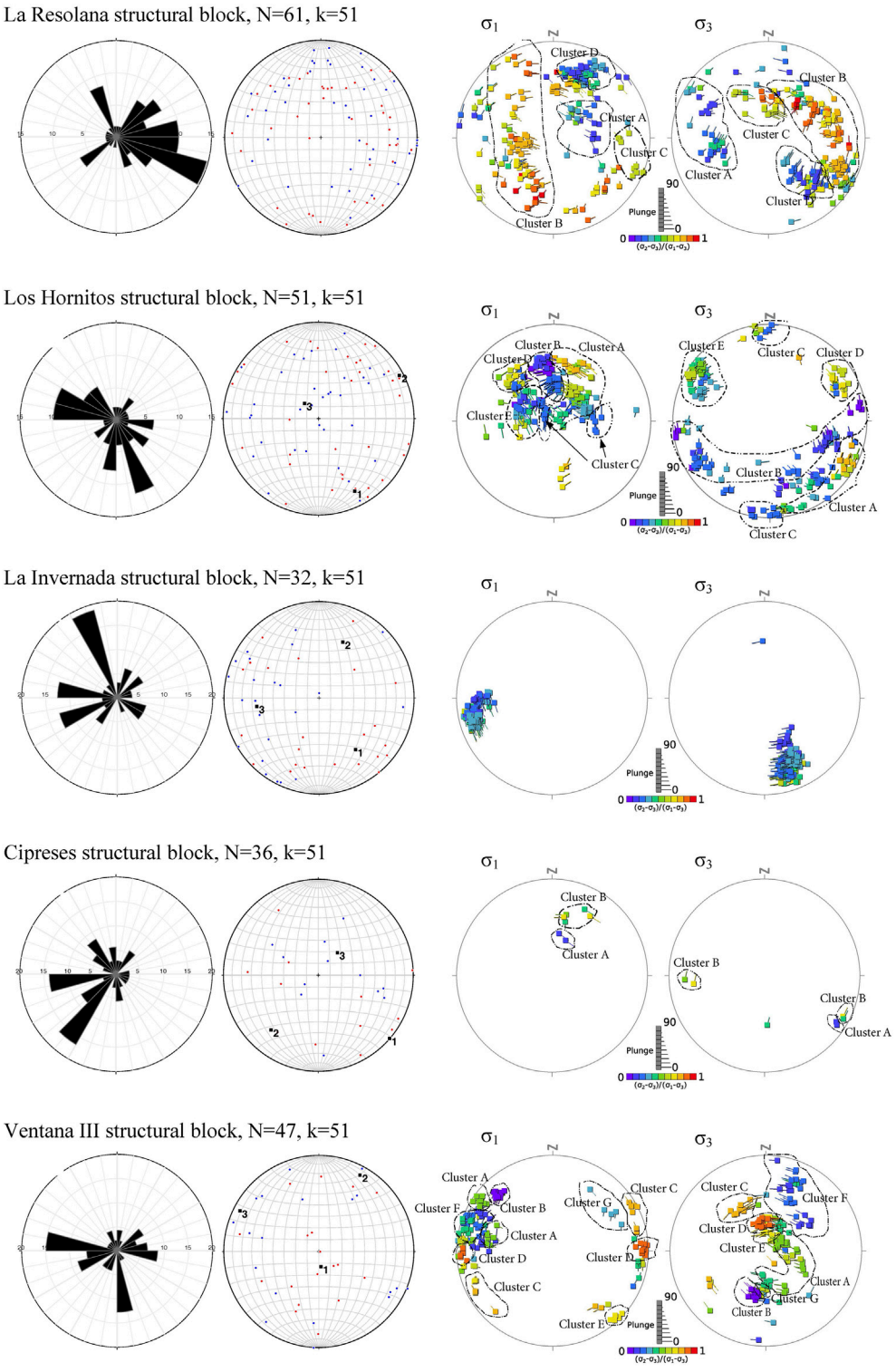

FIGURE 12
Results of the analysis of fault-slip data for 5 structural blocks. For each structural block, the first plot corresponds to a rose diagram for the strike of the fault planes. The second plot shows the P and T axes for each fault plane as blue and red dots respectively, together with the average kinematic axes (1 = stretching, 2 = intermediate, 3 = shortening) in the cases in which deformation is at least moderately homogeneous. The third and fourth plots show the calculated orientations of σ_1 and σ_3 for subgroups of fault-slip data using the Multiple Inverse Method.

ϕ values, with σ_1 plunging at moderate to high angles and σ_3 plunging at low to moderate angles, with its trend varying from ENE to WNW (Figure 12). Cluster C, which is defined by a smaller group of fault planes, can be defined as a purely compressive stress state, with σ_1 subhorizontal and trending ESE, subvertical σ_3 and moderate ϕ values (Figure 12). Finally, Cluster D is characterized by σ_1 plunging at moderate to high angles towards the NE, and σ_3 plunging at low to moderate angles towards the WNW.

4.3.1.2 Los Hornitos structural block

This block is located in and around the Los Hornitos creek, and in its south-eastern area it contains the Los Hornitos monogenetic vents. As in La Resolana, no fault planes were identified cross-cutting the volcanic products of these vents. Consequently, all the 51 fault planes measured in this block cut through rocks of the Colbún Formation. Fault planes show two main preferred orientations (Figure 12): one group strikes predominantly NNW and dips towards the WSW, while another group strikes WNW and dips towards the NNE. A third group, represented by a smaller number of fault planes, strikes N to NNE and dips towards the W (Figure 12).

The kinematic analysis reveals a partially homogeneous deformation, with a subvertical average shortening axis, and a subhorizontal stretching axis trending NNW (Figure 12). These extensional conditions are broadly consistent with the results of the dynamic analysis, in which all the main clusters of σ_1 are subvertical or plunge at high angles, while σ_3 is predominantly subhorizontal, but its trend (and also ϕ values) varies greatly between the different clusters (Figure 12).

4.3.1.3 La Invernada structural block

This block contains exclusively different facies of the LIPC, cropping out in the margins of the La Invernada Lake. Most of the 32 fault planes measured in this block strike NNW, and dip at high angles towards the ENE (Figure 12). Minor groups of faults strike WNW and ENE, both dipping preferentially towards the N.

The kinematic analysis shows a partially homogenous deformation, with pressure axes concentrated in the western quadrants and tension axes concentrated mainly on the SE quadrant (Figure 12). Average shortening axis is E-W and plunging at low to moderate angle towards the W, while the average stretching axis plunges at a similar angle towards the SE. The dynamic analysis reveals a single cluster of principal stresses orientation, with σ_1 subhorizontal and trending ENE, while σ_3 is also subhorizontal and trends NNW (Figure 12). Based on ϕ values, it is possible to distinguish two different stress states, one with ϕ close to 0 (transpressional regime) and one with ϕ close to 0.5 (purely strike-slip regime).

4.3.1.4 Cipreses structural block

Rocks in this structural block are mostly Cretaceous stratified units (Plan de los Yeuques and Colimapu formations), although it also contains minor bodies of the LIPC (monzogranite facies). The statistical analysis of fault plane data (N=36) reveals a preferred NE strike, dipping towards the NW (Figure 12). A second group of faults strike E-W to ENE and dip towards the north, while a third preferred orientation is defined by faults striking NW and dipping towards the NE.

Kinematically, a normal sense of movement prevails (Figure 12), with high-angle pressure axis and a relatively large dispersion of tension axis, although the average stretching axis is subhorizontal and trends SE. The dynamic analysis reveals a small number of solutions, due to the small population of fault planes with kinematic data within this block (N=12). However, it is possible to distinguish two main clusters: for cluster A, σ_1 is inclined at moderate to high angles towards the NNE, σ_3 is subhorizontal and trends WNW, and ϕ values are close to 0. For cluster B, σ_1 also plunges NNE but at lower angles, σ_3 is subhorizontal and varies from WNW to E-W, and ϕ values are between 0.4 and 0.7 (Figure 12).

4.3.1.5 Ventana III structural block

This structural block is located at the SE corner of the study area (Figure 11), around the Ventana creek, and it is composed exclusively by Cretaceous rocks of the Plan de los Yeuques and Colimapu formations. Statistically, two main preferred orientations are observed (N=47): WNW strikes dipping to the NNE, and N-S strikes dipping towards the W. A third, minor group of faults strikes NE to ENE and dips variably to the NW and SE (Figure 12).

Sense of movement of faults in this block is predominantly reverse, and the kinematic analysis shows a partially homogeneous deformation, with a subvertical average stretching axis, and a subhorizontal shortening axis trending WNW (Figure 12). The dynamic analysis reveals a similar result, with most clusters of principal stresses being consistent with a compressive to transpressive regime; σ_3 is predominantly subvertical, while σ_1 is subhorizontal and predominantly trends WNW. However, based on the variations of ϕ values and on the specific orientation of σ_1, it is possible to distinguish several individual stress states, as highlighted in Figure 12.

4.4 Preferred orientations of magmatic bodies and hydrothermal veins

To better understand the link between fault systems and the flow of magmas and hydrothermal fluids, we also analyzed the preferred orientations and geometries of hydrothermal veins, dikes of variable compositions and volcanic morphologies.

A total of 138 hydrothermal veins were measured. The composition of the vein infill is variable; the most commonly observed mineral associations are epidote-chlorite, quartz, biotite, quartz-biotite, tourmaline and calcite. Epidote-chlorite and tourmaline veins commonly display albite haloes. Veins are commonly millimetric, although thicker veins locally occur. They are not related to any kind of known mineral deposit. They cross-cut the LIPC, and some of them also cut through the La Resolana intrusions. In the volcano-sedimentary host rocks, vein intensity is stronger close to the contact with the middle Miocene-Pliocene plutons. From all of this, a middle Miocene-Pliocene age can be inferred for the hydrothermal activity in the study area.

The analysis of preferred orientations (Figure 10) shows three main tendencies. The main preferred orientation is NNW, with variable dip directions. A second preferred orientation is close to E-W, dipping preferentially towards de north. Finally, a third preferred orientation is distinguishable, with veins in this group striking NE and dipping preferentially towards the NW.

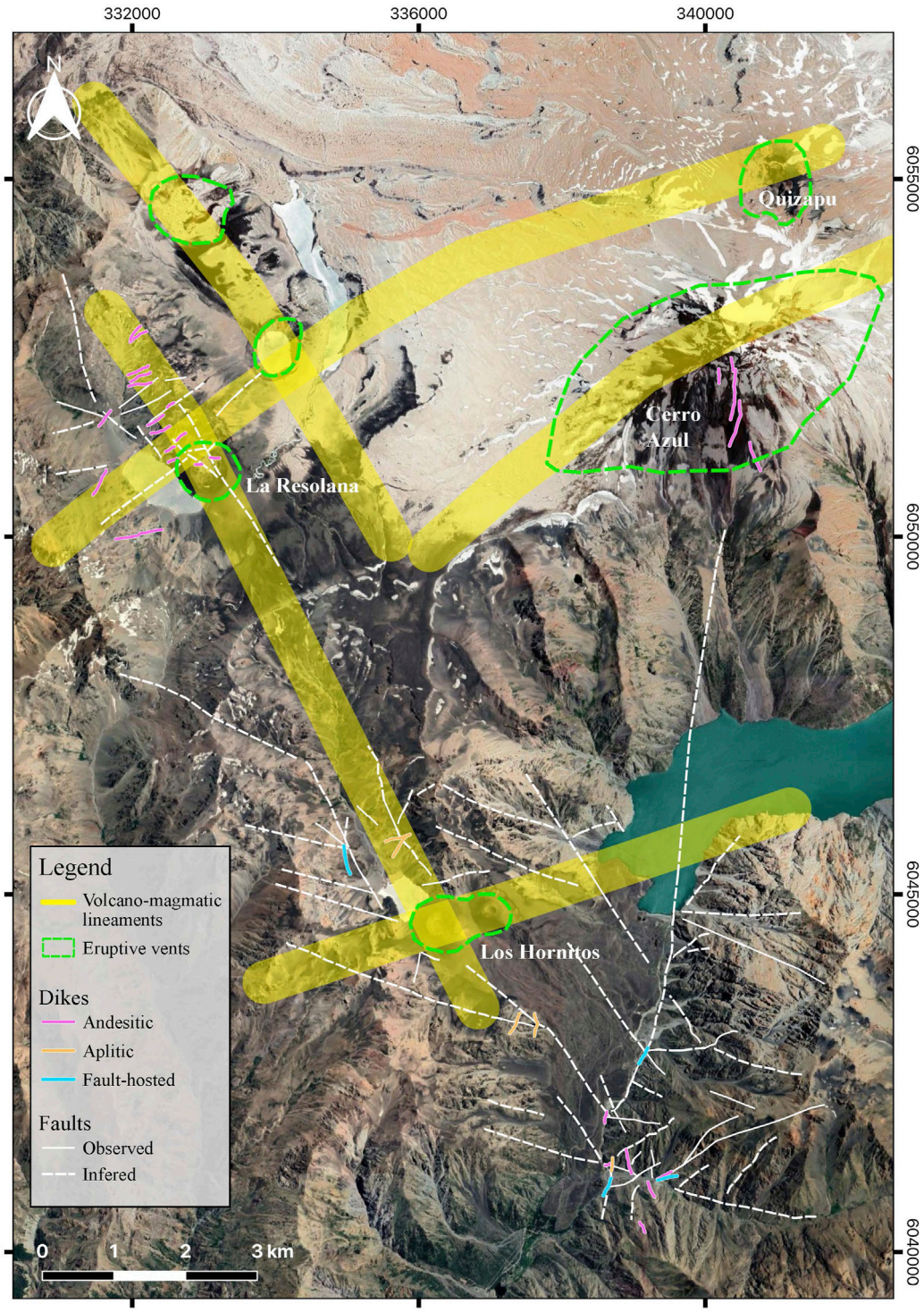

FIGURE 13
Volcanic structures and alignments in the study area.

21 dikes were measured, with predominantly andesitic to dacitic-andesitic compositions, although aplitic dikes were also measured. As with the hydrothermal veins, a late Miocene-Pliocene age is inferred for these dikes due to cross-cutting relationships. The preferred orientation of dikes (Figure 10) highlights two main tendencies. One dike system, striking broadly N-S and dipping at high angles towards the E, was observed at the Ventana III, Cipreses and Los Hornitos areas, while a second dike population strikes predominantly NE and dips towards the NW, observed mainly at La Resolana, and occasionally at Ventana III.

Based on the dikes mapped and measured in the field, complemented with the mapping of additional dike systems and

volcanic morphologies using satellite images, a series of volcano-magmatic lineaments were identified (Figure 13).

The NE-to ENE-striking set of dikes identified at La Resolana, coincides with the elongation direction of the edifice of the Cerro Azul stratovolcano, the distribution of the La Resolana monogenetic vents, and the main crater of the Quizapu volcano (Figure 13). The N-S dike trend, identified mainly around the Cipreses River valley, is also reflected in the orientation of a dike system recognized through satellite images in the southern flank of the Cerro Azul stratovolcano (Figure 13). Finally, when considering the monogenetic vents at both Los Hornitos and La Resolana, a NNW alignment is apparent, coincident with one of the main preferred orientation of faults observed at La Invernada, Los Hornitos and La Resolana (Figures 12, 13).

5 Discussion

5.1 Spatial and temporal geochemical trends in Cenozoic igneous rocks

Understanding the variations of magma chemistry in space and time, can provide crucial information for the interpretation of the tectonic setting of magma generation, ascent and emplacement, and also for the evaluation of the fertility of a magmatic suite, i.e., the capacity of a magma to form a giant porphyry-epithermal system. In particular, a direct relationship has been documented between "adakite-like" magmas and major porphyry-epithermal mineral deposits (Sajona and Maury, 1998; Oyarzún et al., 2001; Richards and Kerrich, 2007; Chiaradia et al., 2009), with these magmas being characterized by features such as high Sr/Y ratios and high HREE/LREE ratios (high slopes in REE diagrams, high La/Yb ratios). Initially, this adakitic signature was interpreted as the product of partial melting of the slab in subduction zones, but subsequently it has been shown that an identical geochemical signature can be obtained through several other processes, including partial melting of subducted sediments, partial melting of an amphibole-garnet bearing lower crust, and/or fractional crystallization of garnet and particularly hornblende during magmatic ascent and emplacement (Richards and Kerrich, 2007; Chiaradia et al., 2009). The observed relationship between adakite-like magmas and giant mineral deposits, has been explained by the highly hydrous character of the magmas generating them, which lead to abundant crystallization of hornblende and the temporal suppression of plagioclase formation, and by their large crustal residence times in thickened continental crust under a compressive tectonic regime (Richards and Kerrich, 2007; Chiaradia et al., 2009; Chiaradia et al., 2012; Chiaradia, 2015; Loucks, 2021). Loucks (2014) proposed the use of these geochemical characteristics to discriminate fertile magmas during mineral exploration.

Here we evaluate the Cenozoic spatial and temporal variabilities of these geochemical parameters in our study area and surrounding region, considering all the available geochemical and geochronological data, both from this work and from a compilation of existing publications (Vergara et al., 1999; Díaz et al., 2020). The rock units considered in our analysis correspond to the Colbún Formation (data from Vergara et al., 1999), the LIPC, the equigranular and porphyritic intrusions of the Brahma porphyry (data from Díaz et al., 2020) and the La Resolana intrusions.

The oldest rocks considered in our compilation belong to the Colbún Formation, which has been subdivided into two units separated by an erosional unconformity (Vergara et al., 1999). The lower unit has K/Ar and $^{40}Ar/^{39}Ar$ ages between 35.2 and 27.4 Ma, while the upper unit has K/Ar ages between 20.3 and 15.4 Ma. The latter strongly overlaps the age range of the Colbún Formation in our study area (Cabezas et al., 2018), and their lithologies are identical. Vergara et al. (1999) also documented the geochemistry and K/Ar ages of subvolcanic intrusions related to the Colbún Formation, with an age range of 35-15 Ma. The volcanic and subvolcanic rocks range in composition from basalt to rhyolite, and most of them show tholeiitic affinity in the AFM diagram (Vergara et al., 1999). In a chondrite normalized REE diagram (Figure 9; Vergara et al., 1999), the Colbún Formation igneous rocks show mostly flat patterns, with almost no enrichment of LREE relative to HREE (La_N/Yb_N ratios of 1–1.5), irrespective of their major elements composition and SiO_2 content. In the fertility diagrams of Loucks (2014; Figure 14) and in adakite-like rocks discriminating diagrams (Figure 14), they plot entirely within the field of normal magmatic arc rocks.

As highlighted before, the intrusive facies of the LIPC (~14-15 Ma) show a calc-alkaline affinity and evidence of HREE depletion, with La_N/Yb_N ratios of 7–11, considerably higher than the partially coeval Colbún Formation. The slope in the REE diagram is slightly higher for the most differentiated (and later) facies. In fertility diagrams, the LIPC facies plot as weakly fertile magmas, while they plot as normal magmatic rocks in the adakite-like discriminate diagrams (Figure 14). All these features are consistent with a progressive increase in the degree of hydration and magma residence times during the evolution of the LIPC, allowing the fractionation of increasing amounts of hornblende.

When our results for the LIPC are compared with the intrusive units related to the nearby and partially coeval Brahma porphyry Cu-Mo deposit, important differences are apparent. Four main intrusive units have been recognized at Brahma (Díaz et al., 2020), two of them equigranular and two porphyritic; all of them have been dated by U-Pb in zircons. The oldest intrusion is a granodiorite (14.6 ± 0.4 Ma), followed by a felsic, hornblende-rich porphyry (14.1 ± 0.2 Ma) and a tonalite (13.4 ± 0.4, 13.8 ± 0.5 Ma). Finally, a second hornblende-rich porphyry was emplaced later (9.3 ± 0.2 Ma). All the intrusive units present at Brahma show steeper slopes in the REE diagram (Figure 9) and show a stronger fertile signature (Figure 14), when compared with the LIPC. The two equigranular units are moderately fertile, the difference with the LIPC being evident in the Sr/Y values (Figure 14). In the adakite-like discriminating plots, the equigranular units still plot in the normal magmatic arc field in the La/Yb versus Yb diagram (La_N/Yb_N 7–19), but they plot in the lower part of the adakite-like rocks in the diagram of Sr/Y versus Y. The two porphyries, in turn, show a similar pattern in terms of REE contents and fertility indices, irrespective of their age difference. They plot entirely within the field of adakite-like rocks (La_N/Yb_N 20–30), and their Sr/Y and V/Sc ratios are characteristic of strongly fertile magmas (Díaz et al., 2020; Figure 14).

Finally, the youngest intrusive units recognized in the study area are the La Resolana intrusions (~4 Ma). This unit is more depleted in HREE (La_N/Yb_N 11.1) and has higher fertility indices than the LIPC (Figures 9, 14), but it is clearly less fertile and less HREE depleted

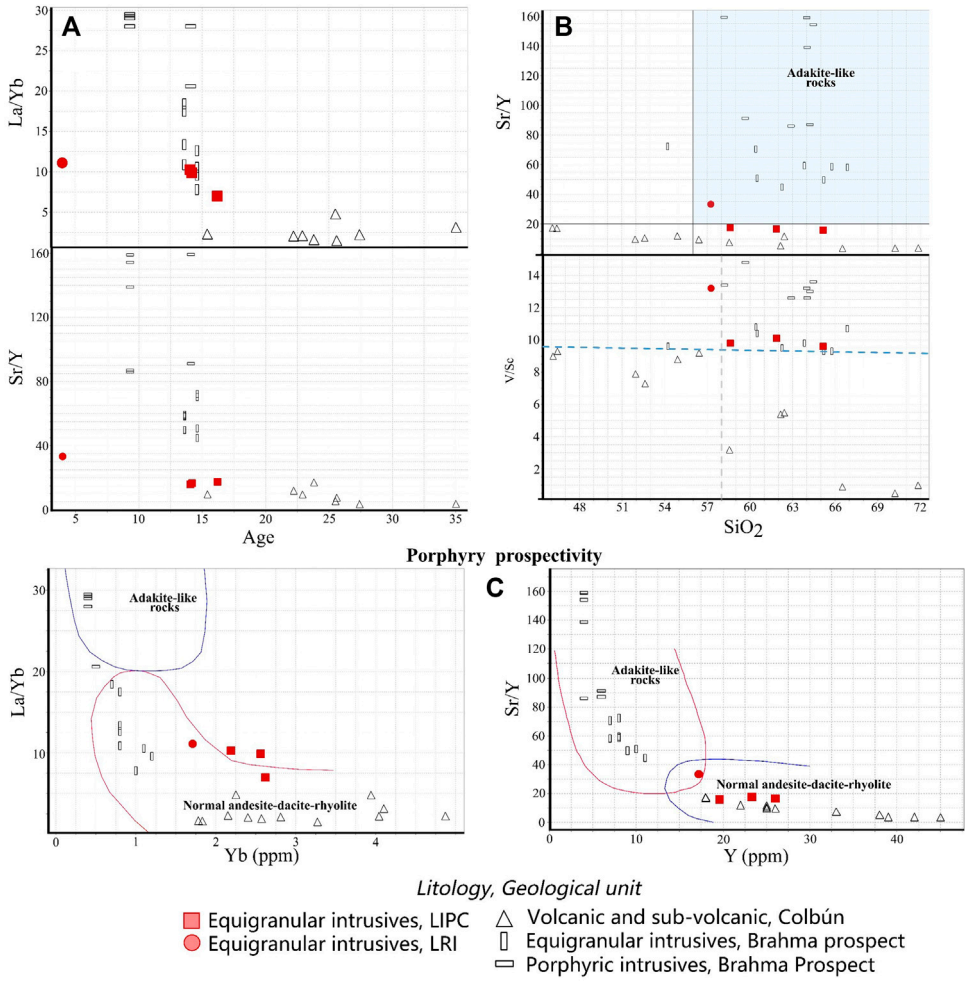

FIGURE 14
Variability of geochemical indices for Mio-Pliocene igneous units of the Principal Cordillera of the Maule Region. **(A)** La/Yb and Sr/Y versus age diagrams. **(B)** Sr/Y and V/Sc versus SiO_2 diagrams. The Adakite-like field in the first plot is from Richards et al. (2012); the blue dashed line in the second plot marks the limit between fertile and barren magmas, according to Loucks (2014). **(C)** Porphyry prospectivity diagrams; the Adakite-like and Normal magmatic arc fields are from Richards et al. (2012).

than any of the Brahma intrusions. It plots within the normal magmatic arc rocks in the La/Yb versus Yb diagram, while in the Sr/Y versus Y diagram it plots in the transition zone between normal magmatic arc rocks and adakite-like rocks.

5.2 Relationship between fault systems and the flow of magmas and hydrothermal fluids

The different fault systems of the study area acted as pathways for the flow of different types of magmas and hydrothermal fluids. In general terms, there is a close correlation between the orientation of fault planes and hydrothermal veins (Figure 10), suggesting a strong structural control on their emplacement. Field mapping demonstrates that many of these veins are syn-tectonic (Figure 3), and that various generations of cross-cutting hydrothermal veins exist in the area. It is likely that hydrothermal fluids were released after the emplacement and progressive crystallization of each of the intrusive facies of the LIPC (~15-12 Ma) and the La Resolana intrusions (~4 Ma). A third hydrothermal pulse is likely to have occurred at ~8-6 Ma, based on the three K-Ar ages obtained by Drake (1976). Our U-Pb zircon ages at the same localities demonstrate that these K-Ar ages do not correspond to crystallization ages, but they likely reflect the occurrence in the area of a major high-temperature hydrothermal alteration event, associated with the emplacement of magmas not exposed at the present-day surface, or cropping out in segments of the LIPC not covered by our fieldwork and sampling. This inferred magmatic-hydrothermal event would be equivalent in age to the Huemul-Risco Bayo plutonic complex (~7.2-6.2 Ma; Schaen et al., 2017), located ~20 km to the south of the LIPC.

The pattern shown by the orientation of dikes seems markedly different than the preferred orientation of fault planes and hydrothermal veins (Figure 10). However, when considering each fault system separately, several correlations are revealed.

The ~NW striking fault systems (WNW to NNW) display evidence of having controlled the emplacement of some of the most differentiated intrusive facies of the study area. Indeed, a syenogranite dike of the LIPC was observed emplaced in a

WNW-striking fault, to the north of the Los Hornitos vents (Figure 7). Also, the La Resolana intrusions show a clear NW elongation (Figure 4), while different felsic facies of the LIPC (monzogranite, granodiorite) display a NW-trending elongation axis (Figure 4). As already discussed, hydrothermal fluids were also channeled by these fault systems, as shown by the WNW and NNW preferred orientations of hydrothermal veins (Figure 10). Finally, these NW-NNW and WNW fault systems can be recognized regionally as morphostructural lineaments in satellite images, and the NW faults in particular, can be correlated to the SE with the Río Maule fault, which is in turn related to the emplacement of the rhyolitic Laguna del Maule volcanic complex (Kohler, 2016), while to the NW, it might be related to the emplacement of NW-elongated Miocene granitoids documented by SERNAGEOMIN (2002) in the Lontué River valley (Figure 1). These high-angle, NW-striking fault systems are oriented at high angles relative to the ~ENE Neogene subduction direction (Somoza, 1998; Somoza and Ghidella, 2012; Bello-González et al., 2018), and also to the ~ENE orientation of σ_1 calculated from the fault planes which cross-cut the different facies of the LIPC (La Invernada structural block, Figure 12), which is responsible for the sinistral-reverse sense of movement of the ~NW-striking faults. This geometric configuration is not ideal for the quick ascent of magmas; instead, it favors a slow ascent and longer residence times, involving the formation of magma chambers in which magmas are allowed to differentiate and volatiles are accumulated, until their sudden release (Cembrano and Lara, 2009; Piquer et al., 2021). It has been proposed that the release of magmas and volatiles along these "misoriented" faults might happen during transient, co- and post-seismic reversals of fault kinematics, during and immediately after major subduction earthquakes (Mpodozis and Cornejo, 2012; Stanton-Yonge et al., 2016). Normal reactivations of NW-striking faults cross-cutting the LIPC observed at the Los Hornitos block, might be associated to this process. Misoriented faults also control magmatism in the Brahma porphyry deposit (Díaz et al., 2020), where a NW to WNW fault system dominates, and the felsic porphyritic intrusions and hydrothermal breccias show a strong NW-WNW elongation.

The ~N-striking faults, in particular the Rio Cipreses fault, exert a strong control on the emplacement of most of the andesitic and daci-andesitic dikes recognized in the field (Figures 3, 10), whose orientation is parallel to the main fault plane (N strike, and high angle dips towards the E). Furthermore, several dikes were emplaced directly along the observed fault planes, evidenced by striated host rocks with growth of syn-tectonic hydrothermal minerals, and by faut gauge zones formed due to post-magmatic reactivations (Figure 3). Towards the north of the La Invernada Lake, satellite image interpretations allow us to identify a set of N-striking dikes at the southern flank of the Cerro Azul volcano (Figure 13), suggesting that the Cipreses fault is acting as one of the feeders of Quaternary volcanism in the study area.

The NE-to ENE-striking faults also exert a strong control on the emplacement of andesitic dikes within the study area (Figure 10). This is particularly evident in the La Resolana area, where a set of andesitic dikes, which intrude the Colbún Formation and some of them cross-cut also the La Resolana intrusions, are parallel to the ENE-to NE-striking faults recognized in the same area (Figure 4). Besides, the Los Hornitos vents show an ENE-trending alignment, the edifice of the Cerro Azul stratovolcano is strongly elongated in a NE to ENE direction, and it is aligned in the same direction with the La Resolana craters (Figure 13), all of which suggest that, as with the Los Cipreses fault, the NE-to ENE-striking structures also play an important role as feeders of ancient and active volcanism in the study area. This fault set is, in theory, the most favorably oriented for magma ascent in this Andean segment, as it is subparallel to the Neogene convergence direction of the Nazca and South American plates (Somoza, 1998; Somoza and Ghidella, 2012; Bello-González et al., 2018), and to the predominant post-middle Miocene maximum compression direction, as shown by the paleo-stress calculations from fault planes cross-cutting the LIPC (Figure 12).

5.3 Controls on spatiotemporal variability of magmatic products

Through an integration of our geochemical and structural interpretations, it is possible to infer the various factors which controlled the fate of Cenozoic magmatic products within the study area: in some cases, relatively primitive magmas were able to reach the surface, while in some other cases, magmas remained stationed in the upper crust, slowly cooling and crystallizing and achieving various degrees of differentiation. Some of these had the capacity to form porphyry Cu-Mo deposits in the vicinity of our study area.

The oldest Cenozoic magmatic rocks within and around our study area, correspond to the Oligocene-early Miocene volcanic and subvolcanic products of the Colbún Formation. As discussed before and as was highlighted by Vergara et al. (1999), the REE patterns, HREE/LREE ratios and fertility indices of these rocks, suggest that they correspond to normal (non adakite-like) magmatic arc rocks, formed under a relatively thin and extended continental crust. Hornblende or garnet fractionation were not significant during magma evolution; instead, magma ascent was rapid and crustal contamination was minimal. Similar patterns have been observed in equivalent volcanic rocks in various segments of the Principal Cordillera of Central and Southern Chile (Charrier et al., 2002; Kay et al., 2005; Piquer et al., 2017). Structural control on volcanism during this period is unclear, as the original geometry of volcanic and subvolcanic rocks has been strongly modified due to subsequent folding, uplift and erosion. It is possible that some of the ENE-striking dikes mapped in the La Resolana block, cross-cutting the Colbún volcanics but not the La Resolana intrusions, correspond to volcanic feeders of the final stages of middle Miocene volcanism. The extensional conditions reflected in our paleo-stress calculations for groups of faults cross-cutting these volcanic rocks, particularly in the Los Hornitos block, likely correspond in part to the preservation of this episode of intra-arc extension in the structural record.

The youngest volcanic products of the Colbún Formation are almost coeval with the oldest facies of the LIPC, and also with the oldest intrusions of the Brahma porphyry (Figure 14). In particular, the biotite granodiorite and the hornblende monzogranite-granodiorite of the LIPC are coeval (within error) with the oldest of the hornblende-rich porphyries of Brahma. However, major geochemical differences are evident when these intrusions are compared (Figs. 9, 14). The LIPC plutons are more depleted in HREE than the host volcanic rocks, but still within the normal range of arc-related calc-alkaline magmas. The coeval porphyritic units at Brahma, in contrast, show a much stronger HREE depletion,

plotting entirely within the field of adakite-like and fertile rocks in discriminating diagrams. Structural mapping and the elongation of intrusive units suggest that in both cases (felsic facies of the LIPC and Brahma porphyries) magmas were channeled by NW-striking fault systems, although the NW-elongation of the magma bodies is more evident for the Brahma porphyries (Díaz et al., 2020). Thus, the higher fertility of the Brahma intrusions is not associated to a regional- or continental-scale control but must be found in another cause.

Variations in REE patterns and fertility indices are commonly inferred to be associated to continental-scale processes: crustal thickening under compression, subduction of oceanic ridges and fracture zones, or subduction and partial melting of sediments and crustal material (e.g., Hollings et al., 2005; Kay et al., 2005; Chiaradia et al., 2009; Piquer et al., 2017). In the case of our study area and the surrounding region, the transition between volcanism of the Colbún Formation and plutonism of the LIPC and Brahma porphyries, might be associated to continental-scale events of crustal thickening and compressive deformation, initiating at ~15-14 Ma. A middle Miocene compressive event, producing folding of Mesozoic and Oligocene-early Miocene stratigraphic units, was already inferred by Spikings et al. (2008), Giambiagi et al. (2012) and Astaburuaga (2014). This change in stress regime is evident from our paleo-stress calculations for specific structural blocks, which shows that when pre-middle Miocene rocks are considered, deformation is heterogeneous, involving various stress states, while for the La Invernada block, which contains exclusively intrusive facies of the LIPC, all faults can be explained by a single stress solution, involving transpressive conditions with subhorizontal, ENE-trending σ_1. These results indicate that these conditions have been the predominant post-middle Miocene stress state. It is important to note that stress states with a ENE to NE orientation of σ_1 are registered in the La Resolana (cluster A) and Ventana III (cluster C) structural blocks. However, the remarkable geochemical differences between the coeval LIPC plutons and the Brahma porphyries, cannot be explained by this continental-scale phenomena. They are better explained by local differences in magma residence times and evolutionary history in magma chambers at different crustal depths, which in turn depend strongly on the orientation of magma pathways relative to the predominant stress tensor. For middle Miocene and later magmatic activity, if magmas are channelled exclusively by NW-striking faults, misoriented relative to the predominant ENE direction of maximum horizontal compression, they will tend to stall at various crustal levels, incorporating crustal material, becoming more differentiated, richer in volatiles, metals and other incompatible elements, and depleted in HREE due to hornblende fractionation. If magma pathways include more favourably oriented faults, magmas will be able to ascend more rapidly, and their adakite-like signatures and fertility indices will be more subdued. This might explain the differences observed between coeval intrusive units emplaced under the same overall tectonic context, separated by only 30 km (Figure 1). Immediately after the emplacement of the adakite-like and strongly fertile Brahma porphyry at 14.1 ± 0.2 Ma, a tonalite was emplaced at ~14-13 Ma, with much weaker fertile signatures (Figure 14), although still higher than the LIPC. Local differences in magma pathways and residence times might also explain this high variability in REE patterns and fertility indices observed within very short periods of time, which would be hard to explain by major changes in subduction parameters or crustal thickness.

This is also consistent with what can be deduced from the structural controls and geochemical characteristics of active volcanism in the study area and surrounding region. As highlighted before, at Los Hornitos, La Resolana and Cerro Azul, ENE-striking faults, parallel to the predominant Neogene compression direction, strongly controlled the emplacement of post-Pliocene dike swarms and also the geometry and distribution of stratovolcanoes (Cerro Azul) and monogenetic vents (Los Hornitos). Magmatic products are primitive (andesites and basaltic andesites), and the compositional zonation observed in olivine phenocrysts at Los Hornitos, has been interpreted as indicative of rapid ascent and limited magma residence times in the crust (Salas et al., 2017). A similar situation was described by Sielfeld et al. (2019) at the Tatara-San Pedro-Pellado volcanic complex, located to the south of the study area (Figure 1), where a major ENE-striking fault system (Tatara Damage Zone) controlled the emplacement of dike swarms and the overall geometry of the volcanic complex and the distribution of minor volcanic vents, as well as the geometry of active geothermal systems. Towards the east, at the Laguna del Maule volcanic complex, Kohler (2016) established that the NW-striking Maule fault controls the distribution of explosive, rhyolitic volcanism, while the NE-striking Troncoso fault allows the ascent of basaltic magma. The products of all these volcanic centres, despite their various degrees of differentiation, show normal magmatic arc chemistry. In contrast, The Nevados de Longaví volcano, located ~60 km to the SW of our study area, constitutes a remarkable anomaly. For equivalent SiO_2 contents, when compared with nearby volcanic centres, it is strongly depleted in HREE, and it shows very elevated La/Yb and Sr/Y ratios, plotting well within the field of adakite-like rocks. Amphibole is abundant in the lavas as phenocryst, irrespective of SiO_2 contents. It can be concluded, then, that the parental magmas of the Nevados de Longaví volcano are a modern equivalent to the strongly hydrated, porphyry-forming magmas present at Brahma and other porphyry Cu deposits elsewhere. It has been hypothesized that the anomaly of the Nevados de Longaví volcanic complex is caused by an abnormal input of fluids from the subducting slab, as the area is located over the projected trace of the subducted Mocha Fracture Zone (Sellés et al., 2004; Rodríguez et al., 2007). However, it is important to note that the Tatara-San Pedro-Pellado volcanic complex, which is of normal magmatic arc composition, is also located over the projection of the same subducted fracture zone (~35 km towards the NE). Without discarding an anomalous input of slab fluids in the area, it is clear that a major role must be played by subsequent magma pathways and evolution, to explain the observed geochemical differences in nearby volcanic centres. This is totally consistent with our interpretations for the variability observed in Miocene intrusions and is a result which has strong implications for mineral exploration, as it demonstrates that magma fertility cannot be extrapolated to an entire metallogenic belt or magmatic arc segment, even when coeval magmatic centres are considered. This is shown by the fact that fertile magmas in Brahma were able to form a porphyry deposit, while the LIPC magmas of the same age (~14 Ma) produced pluton-related alteration zones, but not a porphyry system.

6 Conclusion

Field mapping and petrographic characterization allow us to redefine the La Invernada pluton as a plutonic complex, composed of at least six main intrusive facies, emplaced during a period of ~3 Ma (~15-12 Ma). They are followed by a high-temperature hydrothermal event at ~8-6 Ma, and by the emplacement of the La Resolana intrusions at ~4 Ma. It is confirmed that one of the host rocks of these intrusions correspond to the Cretaceous Plan de los Yeuques Formation.

The initiation of plutonic emplacement and magma differentiation at the LIPC coincides with a major compressive deformation event described in the study area, which is reflected in steeper REE patterns and higher La/Yb, Sr/Y and V/Sc ratios relative to older Cenozoic volcanic and subvolcanic rocks. Fertility indices for the La Resolana intrusions are slightly higher than for the LIPC, however, are still much lower than the values observed in fertile, porphyry-forming magmas in the vicinity of the study area and elsewhere in Central Chile. The strong variability observed in REE compositions and fertility indices between coeval magmas, emplaced in the same arc segment and under the same tectonic parameters, suggest that their differences are better explained by the differences in magma pathways and residence times in the crust. The same conclusion can be deduced from the geochemical differences documented in active volcanic centers in the region around the study area. We propose that a first order role is played by the orientation of the fault system acting as pathway for magma ascent, relative to the orientation of σ_1 (maximum horizontal compression). Our paleo-stress calculations show a strong predominance of ENE-trending σ_1 since the middle Miocene. Under these conditions, NW-striking high-angle faults would be misoriented for reactivation and under high normal stresses, which would slow magma ascent, favoring the formation of magma chambers at various crustal depths, allowing magmas to differentiate, become richer in volatiles, metals and incompatible elements in general, and in which hornblende fractionation will produce HREE depletion and increase magma fertility indices. If this process is particularly efficient, magmas will acquire an adakite-like signature and high fertility indices and will have the potential to form an economic porphyry deposit. In contrast, when magmas are channeled by ENE-to NE-striking faults, subparallel to σ_1, magmas will be able to ascend rapidly, reaching upper crustal levels or even the surface with minimum degrees of differentiation or interaction with crustal material, and forming dike swarms and volcanic alignments of primitive composition. Several intermediate situations are possible, if magma pathways are provided by a combination of misoriented and favorably oriented fault systems, at various crustal levels.

Data availability statement

The original contributions presented in the study are included in the article/Supplementary Material further inquiries can be directed to the corresponding author.

Author contributions

This study was designed by JP with the active collaboration of GP and TF. JP, TF, and FT completed fieldwork and collected samples from the study area. TF and FT completed the structural analysis, paleo-stress calculations and obtained the various fertility and discrimination diagrams, under the supervision of JP. TF completed the petrographic descriptions. JP and TF with the collaboration of GP completed the integrated interpretation of structural, geochemical and geochronological datasets and plots. JP prepared the manuscript, with feedback from TF, FT, and GP. All authors contributed to the article and approved the submitted version.

Funding

All field and analytical work considered for this contribution, was funded by Fondecyt de Iniciación en Investigación project No. 11181048 (ANID, Chile).

Acknowledgments

JP acknowledges support for his research activities from Fondecyt de Iniciación en Investigación project N°11181048 (ANID, Chile) and from Amira Global P1249 project. The regional geology group of SERNAGEOMIN (Chilean National Geological Survey), in particular Carlos Venegas, is acknowledged for highly valuable discussions during different stages of the development of this work, and also for logistical support during one of our field campaigns. Dr. Verónica Oliveros and Dr. Pura Alfonso are sincerely acknowledged for their careful revision of our manuscript.

Conflict of interest

The authors declare that the research was conducted in the absence of any commercial or financial relationships that could be construed as a potential conflict of interest.

Publisher's note

Supplementary material

The Supplementary Material for this article can be found online at: https://www.frontiersin.org/articles/10.3389/feart.2023.1064209/full#supplementary-material

References

Aguirre, L. (1960). *Geología de los Andes de Chile Central, Provincia de Aconcagua*. Santiago: Instituto de Investigaciones Geológicas.

Allmendinger, R. W., Cardozo, N., and Fisher, D. M. (2012). *Structural geology algorithms: Vectors and tensors*. New York: Cambridge University Press.

Astaburuaga, D. (2014). *Evolución estructural del límite Mesozoico-Cenozoico de la Cordillera Principal entre 35o30' y 36oS, región del Maule, Chile*. Undergraduate thesis. Santiago: Universidad de Chile.

Bello-González, J. P., Contreras-Reyes, E., and Arriagada, C. (2018). Predicted path for hotspot tracks off South America since Paleocene times: Tectonic implications of ridge-trench collision along the Andean margin. *Gondwana Res.* 64, 216–234. doi:10.1016/j.gr.2018.07.008

Cabezas, L. M., Muñoz, M., Rojas, M., and Castillo, D. (2018). "Nuevos antecedentes estratigráficos y dataciones radiométricas U-Pb en el valle superior del río Maule a los ~ 35°50'S, Chile central: Implicaciones en la evolución geológica cenozoica," in *XV congreso geológico chileno, concepción, abstracts*, 1101–1104.

Cembrano, J., and Lara, L. (2009). The link between volcanism and tectonics in the southern volcanic zone of the Chilean Andes: A review. *Tectonophysics* 471, 96–113. doi:10.1016/j.tecto.2009.02.038

Cembrano, J., Hervé, F., and Lavenu, A. (1996). The Liquiñe Ofqui Fault Zone: A long-lived intra-arc fault system in southern Chile. *Tectonophysics* 259 (1–3), 55–66. doi:10.1016/0040-1951(95)00066-6

Charrier, R., Wyss, A. R., Flynn, J. J., Swisher, C. C., Norell, M. A., Zapatta, F., et al. (1996). New evidence for late Mesozoic early Cenozoic evolution of the Chilean Andes in the Upper Tinguiririca Valley (35°S), Central Chile. *Journal of South American Earth Sciences* 9, 393–422.

Charrier, R., Baeza, O., Elgueta, S., Flynn, J. J., Gans, P., Kay, S. M., et al. (2002). Evidence for Cenozoic extensional basin development and tectonic inversion south of the flat-slab segment, southern Central Andes, Chile (33°-36° SL). *J. S. Am. Earth Sci.* 15, 117–139. doi:10.1016/s0895-9811(02)00009-3

Chiaradia, M., Merino, D., and Spikings, R. (2009). Rapid transition to long-lived deep crustal magmatic maturation and the formation of giant porphyry-related mineralization (Yanacocha, Peru). *Earth Planet. Sci. Lett.* 288, 505–515. doi:10.1016/j.epsl.2009.10.012

Chiaradia, M., Ulianov, A., Kouzmanov, K., and Beate, B. (2012). Why large porphyry Cu deposits like high Sr/Y magmas? *Sci. Rep.* 2, 685. doi:10.1038/srep00685

Chiaradia, M. (2015). Crustal thickness control on Sr/Y signatures of recent arc magmas: An Earth scale perspective. *Sci. Rep.* 5, 8115. doi:10.1038/srep08115

Contreras, M. A. (2019). *Estudio tefroestratigráfico de los depósitos proximales de los conos piroclásticos "Los Hornitos", Región del Maule, Chile*. Undergraduate thesis. Valdivia: Universidad Austral de Chile.

Díaz, V., Muñoz-Gómez, M., Deckart, K., Townley, B., Mathur, R., and Martínez, O. (2020). The Miocene Brahma porphyry Cu-Mo prospect in central Chilean Andes (35°45′S): Geology, geochronology (U-Pb, Re-Os) and geochemistry. *Ore Geol. Rev.* 122, 103522. doi:10.1016/j.oregeorev.2020.103522

Drake, R. E., Curtis, G., and Vergara, M. (1976). Potassium-argon dating of igneous activity in the central Chilean Andes: Latitude 33°S. *J. Volcanol. Geotherm. Res.* 1, 285–295. doi:10.1016/0377-0273(76)90012-3

Drake, R. E. (1976). Chronology of cenozoic igneous and tectonic events in the central chilean Andes-latitudes 35°30' to 36°S. *J. Volcanol. Geotherm. Res.* 1, 265–284. doi:10.1016/0377-0273(76)90011-1

Giambiagi, L., Mescua, J., Bechis, F., Tassara, A., and Hoke, G. (2012). Thrust belts of the southern Central Andes: Along-strike variations in shortening, topography, crustal geometry, and denudation. *Geol. Soc. Am. Bull.* 124, 1339–1351. doi:10.1130/B30609.1

González, O., and Vergara, M. (1962). "Reconocimiento Geológico de la cordillera de los Andes entre los paralelos 35° y 38°S," in *Publicaciones del Instituto de Geología de la Universidad de Chile 24*, 19–121.

Hildreth, W., and Drake, R. E. (1992). Volcán Quizapu, Chilean Andes. *Bull. Volcanol.* 54, 93–125. doi:10.1007/bf00278002

Hildreth, W., and Moorbath, S. (1988). Crustal contributions to arc magmatism in the Andes of Central Chile. *Contributions Mineralogy Petrology* 98, 455–489. doi:10.1007/bf00372365

Hollings, P., Cooke, D., and Clark, A. (2005). Regional geochemistry of tertiary igneous rocks in central Chile: Implications for the geodynamic environment of giant porphyry copper and epithermal gold mineralization. *Econ. Geol.* 100, 887–904. doi:10.2113/gsecongeo.100.5.887

Irvine, T. N., and Baragar, W. R. A. (1971). A Guide to the chemical classification of the common volcanic rocks. *Can. J. Earth Sci.* 8, 523–548. doi:10.1139/e71-055

Jackson, S. E., Pearson, N. J., Griffin, W. L., and Belousova, E. A. (2004). The application of laser ablation inductively coupled plasma-mass spectrometry to *in situ* U-Pb zircon geochronology. *Chem. Geol.* 211, 47–69. doi:10.1016/j.chemgeo.2004.06.017

Jordan, T. E., Burns, W. M., Veiga, R., Pángaro, F., Copeland, P., Kelley, S., et al. (2001). Extension and basin Formation in the southern Andes caused by increased convergence rate: A mid-cenozoic trigger for the Andes. *Tectonics* 20, 308–324. doi:10.1029/1999tc001181

Kay, S. M., Godoy, E., and Kurtz, A. (2005). Episodic arcmigration, crustal thickening, subduction erosion, and magmatism in the south-central Andes. *Geol. Soc. Am. Bull.* 117, 67–88. doi:10.1130/B25431.1

Klohn, C. (1960). *Geología de la Cordillera de los Andes de Chile Central*. Santiago: Instituto de Investigaciones Geológicas.

Kohler, P. A. (2016). *Geología estructural del Complejo Volcánico Laguna del Maule y su control sobre la deformación cortical activa*. Undergraduate thesis. Concepción: Universidad de Concepción.

Le Maitre, R. W., Streckeisen, A., Zanettin, B., Le Bas, M. J., Bonin, B., Bateman, P., et al. (2002). "Igneous rocks: A classification and glossary of terms," in *Recommendations of the international union of geological sciences subcommission on the systematics of igneous rocks, 2nd edition* (Cambridge: Cambridge University Press).

Lopez-Escobar, L., Cembrano, J., and Moreno, H. (1995). Geochemistry and tectonics of the Chilean southern Andes basaltic Quaternary volcanism (37-46°S). *Rev. Geol. Chile* 22, 219–234. doi:10.5027/andgeoV22n2-a06

Loucks, R. R. (2014). Distinctive composition of copper-ore-forming arc magmas. *Aust. J. Earth Sci.* 61, 5–16. doi:10.1080/08120099.2013.865676

Loucks, R. R. (2021). Deep entrapment of buoyant magmas by orogenic tectonic stress: Its role in producing continental crust, adakites, and porphyry copper deposits. *Earth-Science Rev.* 220, 103744. doi:10.1016/j.earscirev.2021.103744

Lu, Y. J., Loucks, R. R., Florentini, M., McCuaig, T. C., Evans, N. J., and Yang, Z. M. (2016). "Zircon compositions as a pathfinder for porphyry Cu ± Mo ± Au mineral deposits," in *Tectonics and Metallogeny of the Tethyan Orogenic Belt*. Editor J. P. Richards (Littleton, Colorado: Society of Economic Geologists Special Publication) 19, 329–347.

Marret, R., and Allmendinger, R. W. (1990). Kinematic analysis of fault-slip data. *J. Struct. Geol.* 12, 973–986. doi:10.1016/0191-8141(90)90093-e

Mpodozis, C., and Cornejo, P. (2012). "Cenozoic tectonics and porphyry copper systems of the Chilean Andes,". *Geology and genesis of major copper deposits and districts of the world: A tribute to richard H. Sillitoe*. Editor J. W. Hedenquist, et al. (Littleton, Colorado: Society of Economic Geologists Special Publication), 16, 329–360.

Muñoz, M., Tapia, F., Persico, M., Benoit, M., Charrier, R., Farías, M., et al. (2018). Extensional tectonics during late cretaceous evolution of the southern central Andes: Evidence from the Chilean main range at ~35°S. *Tectonophysics* 744, 93–117. doi:10.1016/j.tecto.2018.06.009

Nelson, S. T., Davidson, J. P., and Kowallis, B. J. (1999). Tertiary tectonic history of the southern Andes: The subvolcanic sequence to the tatara-san Pedro volcanic complex, lat 36°S. *GSA Bull.* 11, 1387–1404. doi:10.1130/0016-7606(1999)111<1387:tthots>2.3.co;2

Oyarzun, R., Márquez, A., Lillo, J., López, I., and Rivera, S. (2001). Giant versus small porphyry copper deposits of cenozoic age in northern Chile: Adakitic versus normal calc-alkaline magmatism. *Miner. Deposita* 36, 794–798. doi:10.1007/s001260100205

Petit, J. P. (1987). Criteria for the sense of movement on fault surfaces in brittle rocks. *J. Struct. Geol.* 9, 597–608. doi:10.1016/0191-8141(87)90145-3

Piquer, J., Hollings, P., Rivera, O., Cooke, D. R., Baker, M., and Testa, F. (2017). Along-strike segmentation of the Abanico Basin, central Chile: New chronological, geochemical and structural constraints. *Lithos* 268-271, 174–197. doi:10.1016/j.lithos.2016.10.025

Piquer, J., Sánchez-Alfaro, P., and Pérez-Flores, P. (2021). A new model for the optimal structural context for giant porphyry copper deposit formation. *Geology* 49, 597–601. doi:10.1130/G48287.1

Ramos, V. A., Litvak, V. D., Folguera, A., and Spagnuolo, M. (2014). An andean tectonic cycle: From crustal thickening to extension in a thin crust (34°-37°SL). *Geosci. Front.* 5, 351–367. doi:10.1016/j.gsf.2013.12.009

Richards, J. P., and Kerrich, R. (2007). Special paper: Adakite-like rocks: Their diverse origins and questionable role in metallogenesis. *Econ. Geol.* 102, 537–576. doi:10.2113/gsecongeo.102.4.537

Richards, J. P., Spell, T., Rameh, E., Razique, A., and Fletcher, T. (2012). High Sr/Y magmas reflect arc maturity, high magmatic water content, and porphyry Cu ± Mo ± Au potential: Examples from the tethyan arcs of central and eastern Iran and western Pakistan. *Econ. Geol.* 107, 295–332. doi:10.2113/econgeo.107.2.295

Rodríguez, C., Sellés, D., Dungan, M., Langmuir, C., and Leeman, W. (2007). Adakitic dacites formed by intracrustal crystal fractionation of water-rich parent magmas at Nevado de Longaví volcano (36·2°S; Andean Southern Volcanic Zone, Central Chile). *Journal of Petrology* 48 (11), 2033–2061.

Sajona, F. G., and Maury, R. C. (1998). Association of adakites with gold and copper mineralization in the Philippines. *Comptes Rendus de l'Académie des Sciences - Series IIA - Earth and Planetary Science* 326 (1), 27–34. doi:10.1016/S1251-8050(97)83200-4

Salas, P., Rabbia, O., Hernández, L., and Ruprecht, P. (2017). Mafic monogenetic vents at the Descabezado Grande volcanic field (35.5°S–70.8°W): The northernmost

evidence of regional primitive volcanism in the southern volcanic zone of Chile. *Int. J. Earth Sci.* 106, 1107–1121. doi:10.1007/s00531-016-1357-5

Schaen, A. J., Cottle, J. M., Singer, B. S., Brenhin Keller, C., Garibaldi, N., and Schoene, B. (2017). Complementary crystal accumulation and rhyolite melt segregation in a late Miocene Andean pluton. *Geology* 45, 835–838. doi:10.1130/G39167.1

Sellés, D., Rodríguez, A., Dungan, M., Naranjo, J., and Gardeweg, M. (2004). Geochemistry of Nevado de Longaví Volcano (36.2° S): a compositionally atypical arc volcano in the Southern Volcanic Zone of the Andes. *Revista geológica de Chile* 31 (2), 293–315. doi:10.1130/G39167.1

Servicio Nacional de Geología y Minería [SERNAGEOMIN] (2002). Geological map of Chile: Santiago, SERNAGEOMIN, scale 1: 1,000,000, 3 sheets. digital publication no. 7.

Sielfeld, G., Ruz, J., Brogi, A., Cembrano, J., Stanton-Yonge, A., and Pérez-Flores, P. (2019). Oblique-slip tectonics in an active volcanic chain: A case study from the Southern Andes. *Tectonophysics* 770. doi:10.1016/j.tecto.2019.228221

Sillitoe, R. H. (2010). Porphyry copper systems. *Econ. Geol.* 105, 3–41. doi:10.2113/gsecongeo.105.1.3

Somoza, R., and Ghidella, M. E. (2012). Late Cretaceous to recent plate motions in Western South America revisited. *Earth Planet. Sci. Lett.* 331-332, 152–163. doi:10.1016/j.epsl.2012.03.003

Somoza, R. (1998). Updated azca (Farallon)—south America relative motions during the last 40 My: Implications for mountain building in the central andean region. *J. S. Am. Earth Sci.* 11, 211–215. doi:10.1016/S0895-9811(98)00012-1

Spikings, R., Dungan, M., Foeken, J., Carter, A., Page, L., and Stuart, F. (2008). Tectonic response of the central Chilean margin (35-38°S) to the collision and subduction of heterogeneous oceanic crust: A thermochronological study. *J. Geol. Soc. Lond.* 165, 941–953. doi:10.1144/0016-76492007-115

Stanton-Yonge, A., Griffith, W. A., Cembrano, J., Julien, St.R., and Iturrieta, P. (2016). Tectonic role of margin-parallel and margin-transverse faults during oblique subduction in the Southern Volcanic Zone of the Andes: Insights from boundary element modeling. *Tectonics* 35, 1990–2013. doi:10.1002/2016TC004226

Suarez, M., and Emparan, C. (1995). The stratigraphy, geochronology and paleophysiography of a Miocene fresh-water interarc basin, southern Chile. *J. S. Am. Earth Sci.* 8, 17–31. doi:10.1016/0895-9811(94)00038-4

Sun, S. S., and McDonough, W. F. (1989). Chemical and isotopic systematics of oceanic basalts: Implications for mantle composition and processes. *Geol. Soc. Spec. Publ.* 42, 313–345. doi:10.1144/GSL.SP.1989.042.01.19

Tapia, F., Farías, M., Naipauer, M., and Puratich, J. (2015). Late Cenozoic contractional evolution of the current arc-volcanic region along the southern Central Andes (35°20'S). *J. Geodyn.* 88, 36–51. doi:10.1016/j.jog.2015.01.001

Tassara, A., and Echaurren, A. (2012). Anatomy of the andean subduction zone: Three-dimensional density model upgraded and compared against global-scale models. *Geophys. J. Int.* 189, 161–168. doi:10.1111/j.1365-246X.2012.05397.x

Torres, J. (2021). *Caracterización del lineamiento Laguna fea-volcán san Pedro, región del Maule: Relación con actividad magmática e hidrotermal*. Undergraduate thesis. Valdivia: Universidad Austral de Chile.

Vergara, M., Morata, D., Hickey-Vargas, R., López-Escobar, L., and Beccar, I. (1999). Cenozoic tholeiitic volcanism in the Colbún area, Linares precordillera, central Chile (35°35'-36°S). *Rev. Geol. Chile* 26 (1), 23–41.

Williams, I. S. (1998). "U–Th–Pb geochronology by ion microprobe," in *Applications of microanalytical techniques to understanding mineralizing processes*. *Reviews in economic geology*. Editor M. A. McKibben, et al. 7, 1–35.

Yamaji, A. (2000). The multiple inverse method: A new technique to separate stresses from heterogeneous fault-slip data. *J. Struct. Geol.* 22, 441–452. doi:10.1016/S0191-8141(99)00163-7